Theory of Plasticity and Strain Hardening of Glassy Polymers

Thomas C. Merlette, Jeirome Hem, Caroline Crauste-Thibierge, Sergio Ciliberto, Florence Clement, Paul Sotta, Didier R Long

Theory of plasticity and strain hardening of glassy polymers

Thomas C. Merlette,[†] Jérôme Hem,[‡] Caroline Crauste-Thibierge,[‡] Sergio Ciliberto,[‡] Florence Clément,[†] Paul Sotta,[†,¶] and Didier R. Long*[,†,§]

[†]*Laboratoire Polymères et Matériaux Avancés, CNRS/Solvay, UMR 5268, 87 avenue des Frères Perret, 69192 Saint Fons Cedex, France*

[‡]*ENSL, CNRS, Laboratoire de Physique, UMR 5672, F-69342 Lyon, France*

[¶]*Univ Lyon,CNRS, INSA Lyon, Université Claude Bernard Lyon 1, IMP, UMR5223, 69100 Villeurbanne, France*

[§]*Univ. Lyon, CNRS, INSA Lyon, Université Claude Bernard Lyon 1, MATEIS, UMR5510, 69100 Villeurbanne, France*

E-mail: didier.long@insa-lyon.fr

June 23, 2023

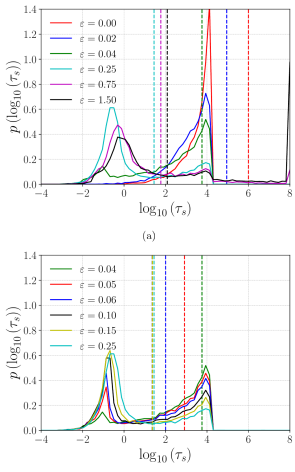

Abstract

We extend a theory for the deformation of glassy polymers based on the heterogeneous nature of the dynamics up to the strain hardening regime. We attribute the latter to the increase of free energy barriers for α-relaxation as a consequence of local orientation of monomers. The free energy barriers are set on a scale $\xi \approx 5$ nm or of about $N_c \sim 1000$ monomers which is involved in the α-relaxation mechanism. The variation of the local free energy barriers is given by the expression $\Delta F(\underset{\sim}{\sigma}, \underset{\sim}{q}) = \Delta F_0 - \frac{\xi^3 \underset{\sim}{\sigma}:\underset{\sim}{\sigma}}{2G_0'} + \tilde{\mu}_2 \cdot N_c \cdot Tr(\underset{\sim}{q}^2)$ where ΔF_0 is the free energy barrier per monomer in the glassy state, typically $\sim 40 - 45 k_B T_g$ for an aged polymer, $\underset{\sim}{q}$ is the local order parameter (nematic in nature) whose distribution is computed during the course of deformation, $\underset{\sim}{\sigma}$ is the local stress and G_0' is the bulk glassy modulus. $\tilde{\mu}_2$ is an energy scale of typical order 0.2-0.3$k_B T_g$. The second term is negative and is responsible for yielding and the onset of plastic flow. The third one is positive and becomes important after a large deformation has significantly oriented the chains on the scale of the monomers. It may overcompensate the decrease of the free energy barriers due to the increasing stress and is responsible for strain hardening. Since the contribution of the stress to the reduction of the free energy barrier between stress softening and the deformation $\lambda \sim 2$ is of the order of $-5 k_B T_g$, the contribution which leads to strain hardening, $\tilde{\mu}_2 \cdot N_c \cdot Tr(\underset{\sim}{q}^2)$, is found to be of the order of 10 $k_B T_g$ which corresponds to an increase of the order of $0.01 k_B T_g$ per monomer. This order of magnitude is compatible with the calculated values of the order parameter $q \sim 0.3$ in the direction of tension during our simulations as well as that measured by Vogt et al (1990) by NMR. We calculate the evolution dynamics of the order parameter $\underset{\sim}{q}$. Its dynamics is controlled by a driving force due to the local stress and a relaxation process due to rotational diffusion. The latter is entropic in nature and may be very slow in glassy polymers. We compare the predictions of our model to recent experimental results regarding both the evolution of the dominant relaxation time under applied strain and that of the width of the relaxation times distribution up to large deformation amplitude, and more specifically their non-monotonic behavior.

I. Introduction

The mechanical and dynamical properties of glassy polymers have been intensively studied for a long time, due to their fundamental and technological importance.[1] Glassy polymers exhibit a maximum in the stress-strain curves (yield point) at a strain value of a few percents and a typical yield stress value of a few tens of MPa's,[1,2] followed by the so-called stress softening regime corresponding to a decrease of the stress of the order of a few (up to typically ten) MPa's, depending on the thermo-mechanical history of the sample.[3] This regime is followed by a stress plateau corresponding to plastic flow. Strain hardening may then occur at even larger strain values. This regime corresponds to a roughly linear increase of the stress as a function of the strain, with a slope G_R of typical order of magnitude 10^7-10^8 Pa well below the glass transition.[4,5] Strain hardening, which is enhanced in polymers with large molecular weights,[4,6] is essential for obtaining high mechanical properties, since it prevents strain localization and the propagation of cracks or the formation of shear bands,[6–9] thereby making the polymer ductile and tough.

On the microscopic scale, an essential feature of polymers in the glassy state is the strongly heterogeneous nature of the dynamics[10,11] on a scale ξ of 3 to 5 nm as measured by NMR[12] or deduced by fluorescence recovery after photo-bleaching (FRAP).[13] The corresponding distribution of relaxation times (DRT) has been shown to span up to eight decades.[14–16] Loo et al, Ediger et al, Kalfus et al, and Ciliberto et al[17–28] have studied the dynamics under plastic deformation by NMR, reorientation dynamics of small fluorescent molecular probes and dielectric spectroscopy, respectively. The dynamics is accelerated even before yield up to the stress softening regime and the onset of plastic flow. Conversely, the dominant relaxation time τ_α increases in the strain hardening regime.[18–20,26–28] It was also observed that the evolution of the width of the DRT is non-monotonic. The width first decreases, then reaches a minimum at the end of the stress softening regime and increases again in the strain hardening regime. These non-monotonic evolutions of τ_α and of the width of the DRT appear to be key features of strain hardening. Hem et al[27,28] attributed the increase

of the stress in the strain hardening regime to the increase of the dominant relaxation time τ_α. Indeed, the measured increase of the stress in the strain hardening regime is consistent with the increase of the monomer relaxation time τ_α. It was argued by Hem et al[27,28] that this increase of the relaxation time may account for an additional contribution to the flow stress of the order of $\sigma_{hard}(\varepsilon) = G_0'(\tau_\alpha(\varepsilon) - \tau_{soft})\dot{\varepsilon}$ where ε (resp. $\dot{\varepsilon}$) is the strain (resp. strain rate), τ_{soft} is the α-relaxation time at the end of the stress softening regime (where it is comparatively faster) and G_0' is a high frequency (glassy) shear modulus of the order of 10^9 Pa. This interpretation is consistent with the conclusions of Hoy and Robbins who attributed strain hardening to molecular mechanisms similar to those which control the yield stress and the flow stress.[7,29–33] These new results rule out the picture of entropic elasticity associated to entanglements proposed by Haward.[34]

Mechanical properties of polymer glasses have also been studied by molecular dynamics (MD) simulations.[35–41] However, unraveling the processes involved in plasticity and strain hardening by molecular dynamics simulations remains elusive though the studies by Robbins, Hoy and Ge brought some new insights regarding the mechanisms related to strain hardening.[29,31,42,43] Chen and Schweizer have described the plastic onset, yield and plastic flow of glassy polymers within the Non-linear Langevin Equation model, an approach conceptually similar to that of the energy landscape.[44–47] Note that the spatial aspect of the problem is not explicit in this mean-field description which lacks an explicit 3D description. At small deformation, the position of the system is slightly higher in the landscape than at rest, resulting in an accelerated dynamics. When stress is released, the system goes back down to its initial state. At higher strain, the free energy barriers are tilted and the system starts to flow. On the other hand, Dequidt et al[48,49] have proposed that the decrease of the barriers is quadratic in the applied stress and scales like a quadratic invariant of the stress tensor $-\underset{\sim}{\sigma}:\underset{\sim}{\sigma}$,[49,50] the reduction corresponding to the stored elastic energy on the scale $\xi \sim 3-5$ nm. Based on this assumption, they proposed a model to calculate the evolution of the DRT in

3D under any thermomechanical histories in the linear and plastic flow regime, but without strain hardening. An important difference between these two approaches is the scale involved in the α-relaxation process: Dequidt et al assume that this scale involves about $N_c \sim 1000$ monomers[14,49] whereas Schweizer et al consider cages of the order of 10 monomers.[44] The physical mechanisms introduced by Dequidt et al[49–51] have been confirmed quantitatively by Belguise et al by a detailed comparison of the stress relaxation function obtained experimentally in the small amplitude plastic deformation regime to the predictions of the model.[52]

Other key features of glassy polymers in the strain hardening regime are memory effects, commonly referred to as Bauschinger effect.[42,43,53,54] When the deformation is stopped at some point during strain hardening and resumed after some waiting time, the second stress-strain curve superposes on the reference one obtained at constant strain rate all along.[42,43,53,54] Various histories of deformation in the strain hardening regime have also been considered in studies aimed at quantifying the microscopic dynamics.[18–20,26–28] It was observed that the dominant relaxation time increased rapidly when arresting the deformation, then decreased back rapidly as well upon resuming the deformation before rejoining that of the reference test. These memory effects were interpreted by Hem et al[28] as the consequence of changes in the free energy barriers for α-relaxation induced by the deformation applied to the sample. It was proposed that these changes are the sum of two contributions. The first one is negative and scales like the quadratic invariant $-\underset{\sim}{\sigma}:\underset{\sim}{\sigma}$ introduced by Dequidt et al[48–52] for describing yield stress and plastic flow in the absence of strain hardening. This contribution relaxes with the stress, which can be very fast. The second contribution is positive and is responsible for strain hardening.[28,55] It is a function of chain orientation at the monomer level, which may relax very slowly, with an associated relaxation time possibly of the order of days, weeks or even more, depending on temperature and on the dynamical state, itself resulting from the thermomechanical history, of the sample. Hem et al have argued that Bauschinger memory effects[43,53] could be explained by the slow relaxation of

the structural change, on much longer time-scales than the one associated to the stress and to the experimental time-scales.

In this manuscript, we introduce new physical mechanisms to account for strain hardening. By analogy to the model of Chen and Schweizer,[46] we assume that monomers are oriented by the deformation, which is essentially homogeneous at the length scale ξ. This slows down the local dynamics by strengthening interactions between monomers, as free energy barriers are enhanced by local chain alignment on the monomer scale, in addition to the effect of the stress,[49–51] as was discussed by Hem et al.[28] Though the system remains far from full alignment, i.e. far from an isotropic-nematic transition, we introduce a second rank tensor order parameter analogous to a tensorial nematic order parameter. The evolution of this order parameter is described by a dynamical equation. When the stress is set to zero, the order parameter relaxes towards the isotropic state, though this relaxation may be long on the considered time-scale. Besides strain hardening itself, which is studied here in a systematic way, the proposed extension of the model accounts for various effects which are distinctive of glassy polymers, namely the complex evolution of the dominant relaxation time and of the width of the DRT, from the linear elastic regime of deformation up to the strain hardening regime.

II. Theory for plastic flow of glassy polymers

II.1. Summary of the current state of the theory

Let us first summarize the theory previously developed in references.[14,28,48–51,56,57] Long and Lequeux,[56] and Merabia and Long[14,58] have proposed that the α-relaxation process involves a number $N_c \sim 1000$ monomers, which corresponds to a scale of about 5 nm. The local relaxation time is determined by density fluctuations. Slow subunits correspond to upwards density fluctuations of the order of 1 to 2%, while fast subunits correspond to downwards

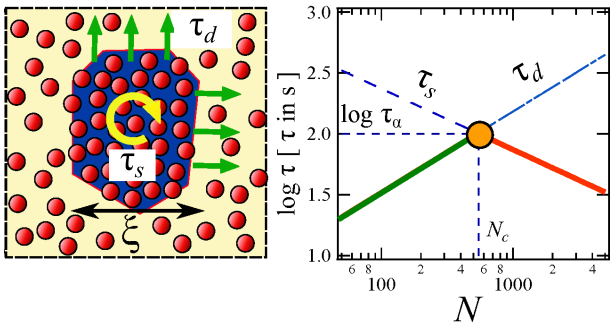

Figure 1: Left: A slow (high density) subunit of size $\xi \sim 3-5$ nm within a faster (lower density) surrounding may relax either by internal free volume reorganization (time τ_s) or diffusion (time τ_d) (density differences are exagerated). Right: variation of τ_s (dashed curve) and $\tau_d \sim N^{2/3}$ (dash-dotted curve) vs the number N of monomers in subunits. The smaller the scale, the larger the density fluctuations, hence the larger the value of τ_s. On the other hand, the smaller the scale, the shorter the lifetime τ_d of density fluctuations.

density fluctuations of the order of -1 or -2%.

The size ξ of dynamical heterogeneities corresponding to the dominant scale of the α-relaxation process stems from two competing relaxation processes.[14] The first one corresponds to reallocation of local free volume at the length scale 5 nm, within the standard free volume picture on this local scale. The smaller the scale, the larger the density fluctuations. In principle, one could find increasingly slower subunits by considering decreasing scales. On the other hand, the smaller the scale, the shorter the lifetime of a density fluctuation, as the local density can relax by free volume diffusion from the neighboring fast, less dense subunits. Fast dynamical states can thus diffuse from fast neighboring subunits. This process has been called facilitation mechanism.[14,45,51,58–60] The number N_c of monomers involved in the α-relaxation process is thus determined by considering the lifetime τ_d of density fluctuations (see Figure 1).[14,58] Therefore, the corresponding length scale $\xi = aN_c^{1/3}$ (a is a monomer length) is the smallest scale at which the lifetime of density fluctuations can be equal to or larger than τ_α. Density fluctuations on smaller scales are irrelevant for the α-relaxation process, being too short-lived. As a consequence of the facilitation mechanism,

the relaxation time τ_α obeys the following relation

$$\tau_\alpha = \tau_d = N_c^{2/3}\tau_f \tag{1}$$

where the characteristic relaxation time of fast subunits τ_f obeys:

$$\int_0^{\tau_f} Q(\tau)d\tau = q_c \tag{2}$$

in which $Q(\tau)$ is the distribution of relaxation times (DRT) and the fraction q_c of fast subunits is an adjustable parameter, typically a few tens of percents. The lifetime of density fluctuations τ_d can be considered as a melting time of large density fluctuations by the fastest surrounding subunits.[14,58] The relation $\tau_d = N_c^{2/3}\tau_f$ means that the relaxation of the slowest subunits corresponds to both internal processes and to the melting by the faster environment. Equation (2) is key for calculating the melting kinetics of a glassy polymer upon heating.[58] In reference,[58] Merabia and Long have shown that the rejuvenation dynamics as measured by Kovacs[61] can be correctly described by using the value $q_c = 0.3$. The dominant relaxation time τ_α can never be larger than τ_d as a consequence of the facilitation mechanism. This mechanism is responsible for the narrowing of the distribution of relaxation times under applied strain up to the stress softening regime.[18,27,28,50,51] Note that so-called facilitation mechanisms, according to which the local dynamics also depends on the dynamics of the neighbors, have also been introduced in different contexts.[59,60]

In the presence of a local stress $\underset{\sim}{\sigma}$, before strain hardening takes place, Dequidt et al[48,49] and Conca et al[51] have proposed that the α-relaxation is an activated process with free energy barriers given by

$$\Delta F(\underset{\sim}{\sigma}, T, \rho) = \Delta F_0(T, \rho) - \frac{\xi^3 \underset{\sim}{\sigma} : \underset{\sim}{\sigma}}{2G_0'} \tag{3}$$

where $\xi^3 = N_c a^3$ is the scale of dynamical heterogeneities, with a number $N_c \sim 1000$ of monomers involved in α-relaxation and $a \sim 0.5$ nm a monomer size. $\Delta F_0(T, \rho)$ is the free energy barrier for the polymer at rest at temperature T and density ρ before the stress has been applied, and is typically of the order of $\sim 40{-}45 k_B T_g$ for an aged polymer. The quantity $\underset{\sim}{\sigma} : \underset{\sim}{\sigma}$ is the quadratic invariant defined as $\underset{\sim}{\sigma} : \underset{\sim}{\sigma} = (1/2)\left[(\sigma_1 - \sigma_2)^2 + (\sigma_2 - \sigma_3)^2 + (\sigma_3 - \sigma_1)^2\right]$ where $\sigma_1, \sigma_2, \sigma_3$ are the eigenvalues of the local stress tensor $\underset{\sim}{\sigma}$. In shear deformation along direction 1 with a displacement gradient along direction 2, this invariant is equal to $3\sigma_{12}^2$. In the course of plastic deformation, subunits relax randomly and the local relaxation time of a given subunit becomes a complex quantity which depends on temperature, on the local state (ρ, $\underset{\sim}{\sigma}$), on the history of relaxation and on the aging process undergone by the considered subunit.[49,51,58]

For large deformation amplitudes, Hem et al[28] have argued that, for polymers which experience strain hardening, monomer orientation contributes to increasing free energy barriers, which become

$$\Delta F(\underset{\sim}{\sigma}, T, \rho) = \Delta F_0(T, \rho) - \frac{\xi^3 \underset{\sim}{\sigma} : \underset{\sim}{\sigma}}{2G_0'} + N_c \kappa(\varepsilon) \tag{4}$$

where ε is the strain. This is of course a short-hand notation since the orientation depends on the whole deformation history and relaxes, at least partially, during the applied deformation. We will define $\kappa(\varepsilon)$ and calculate its evolution for each subunit as a function of the deformation history.

II.2. Local tensorial order parameter

Upon applying a deformation on a polymer, the microscopic deformations on short timescales may be assumed to be affine: the small tensorial deformation applied on the macroscopic scale is the same down to the molecular scale, before relaxation takes place.[62] Figure 2 illustrates how deformation results in local monomer orientation. At high temperature,

this orientation is short-lived because relaxation on the monomer scale is very fast. Below T_g, this orientation may be long-lived because monomer relaxation times during plastic flow may be as large as 10^3 to 10^4 s.[26–28] As a consequence, monomer orientation may increase during deformation. We will calculate this evolution in the following.

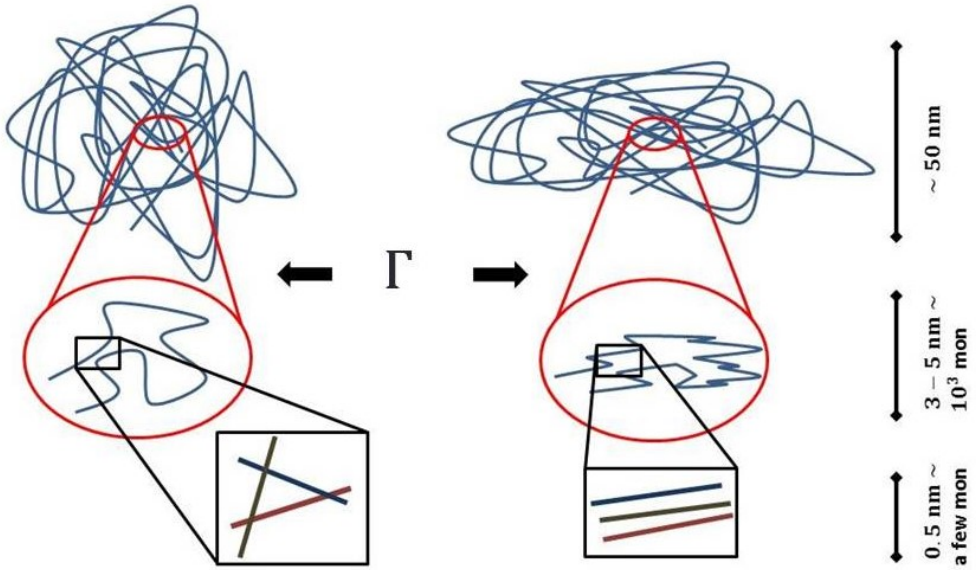

Figure 2: Schematics suggesting how deformation affects the local configurations. At large length scales, polymer chains maintain their Gaussian structure. At the scale of dynamical heterogeneities, monomers partially align in the direction of deformation because segmental relaxation is too slow. As a consequence, intermolecular interactions and correlations are enhanced, reducing the local mobility and slowing down the dynamics.

Let us consider one monomer bond, described by a unit vector $\vec{u}$. When an infinitesimal deformation tensor $\underset{\sim}{I_d} + \underset{\sim}{\kappa}$ is applied, where $\underset{\sim}{I_d}$ is the identity tensor and $\underset{\sim}{\kappa}$ a small strain tensor, the bond vector of coordinates u_i becomes

$$u_i' = u_i + \kappa_{i,j} u_j$$

where summation over repeated indices is implicit. Note that we assume here that monomers can be slightly extended by the applied strain, which is possible if so-called monomers are actually coarse-grained chemical units, beyond one Kuhn segment. Up to linear order, one

gets

$$\langle u'_i u'_l \rangle = \langle u_i u_l \rangle + \langle \kappa_{i,j} u_j u_l + \kappa_{l,m} u_m u_i \rangle$$

where the average $\langle . \rangle$ is performed over the N_c monomers in a given subunit of size ξ. Since the initial state is isotropic, one has $\langle u_i u_j \rangle = \frac{1}{3}\delta_{i,j}$ and

$$\langle u'_i u'_l \rangle = \frac{1}{3}\delta_{i,l} + \frac{1}{3}\left(\kappa_{i,l} + \kappa_{l,i}\right)$$

The local order parameter $\underset{\sim}{q}$ is defined by

$$q_{i,j} = \frac{1}{2}\left\langle 3u'_i u'_j - \delta_{i,j} \right\rangle \tag{5}$$

which yields:

$$q_{i,j} = \frac{1}{2}\left(\kappa_{i,j} + \kappa_{j,i}\right) \tag{6}$$

that is $\underset{\sim}{q} = (1/2)\left(\underset{\sim}{\kappa} + \underset{\sim}{\kappa}^t\right)$, where $\underset{\sim}{\kappa}^t$ is the transpose of $\underset{\sim}{\kappa}$. This equation relates the local (quadrupolar) orientational order parameter $\underset{\sim}{q}$ to the local deformation tensor $\underset{\sim}{\kappa}$. In the Supplementary Information document, we consider the case where monomers are described as inextensible, rigid rods. We show that this results in an equation essentially similar to Equation (6), within a prefactor 0.6.

II.3. Impact of monomer orientation on energy barriers

We assume that the orientation of the chains on the monomer scale leads to an increase of their molecular interaction. This is due to the anisotropy of van der Waals interactions. Quadrupolar polarization along the backbone is generally larger than in a direction normal to the backbone, which may lead to nematic ordering when the difference is sufficiently large.[63] The interaction energy is a quadratic function of the local order parameter, is invariant by frame rotation and is negative. It may thus be assumed to be proportional to $-Tr\left(\underset{\sim}{q}^2\right)$,

where $\underset{\sim}{q}$ is the tensorial order parameter defined in Equation (5). As a consequence, the interaction energies of the monomers decrease (they increase in absolute value) under the applied deformation. The latter tends indeed to orient the monomers and to produce hairpins along the backbone. We assume that full alignment would lead to a decrease (an increase in absolute value) of the interaction energy of the order of -0.2 to $-0.3k_BT$ per monomer. This interaction energy is smaller in absolute value than, but nevertheless of the same order of magnitude as, the value which would lead to nematic ordering.[63] Thus the decrease of free energy per monomer is given by $-\tilde{\mu}_2 Tr\left(\underset{\sim}{q}^2\right)$, where $\tilde{\mu}_2$ is typically of the order of 0.2 to $0.3k_BT_g$. Our point of view is that, for a significantly larger anisotropy of the interactions (that is, a significantly larger $\tilde{\mu}_2$ value), the polymer would be in a nematic state, corresponding to a liquid crystalline polymer,[63–65] while for a significantly smaller anisotropy, there would be no strain hardening at all, as we shall see in the following.

The next issue is to elucidate the effect of this decrease (increase in absolute value) of interaction energies between monomers on the free energy barriers for α-relaxation. The monomers are driven in a lower energy state which is not favorable for the random motions leading to α-relaxation. We assume that, in order to be able to explore the whole phase space for α-relaxation attempts, the monomers need to recover their initial (closer to equilibrium) state of random orientation. This can be made at a cost of $\tilde{\mu}_2 N_c Tr\left(\underset{\sim}{q}^2\right)$ per dynamical subunit. The free energy barriers are thus increased by this amount.

It follows that the local free energy barrier for α-relaxation is modified into :

$$\Delta F(\underset{\sim}{\sigma}, \underset{\sim}{q}) = \Delta F_0 - \frac{\xi^3 \underset{\sim}{\sigma} : \underset{\sim}{\sigma}}{2G_0'} + \tilde{\mu}_2 N_c Tr\left(\underset{\sim}{q}^2\right) \tag{7}$$

The term $N_c\tilde{\mu}_2 Tr\left(\underset{\sim}{q}^2\right)$ may be rewritten $k_BT\mu_2 Tr\left(\underset{\sim}{q}^2\right)$ with $\mu_2 = N_c\tilde{\mu}_2/k_BT$ a dimensionless, adjustable parameter of the model that we predict to be of the order of 200-300

typically, as we shall see below.

From equation (7), the evolution of the local relaxation time τ can be written:

$$\tau = \tau_0 \exp\left(\frac{\Delta F(\underset{\sim}{\sigma}, \underset{\sim}{q})}{k_B T}\right) = \tau_0 \exp\left(\frac{\Delta F_0}{k_B T} - \lambda \underset{\sim}{\sigma} : \underset{\sim}{\sigma} + \mu_2 Tr\left(\underset{\sim}{q}^2\right)\right) \quad (8)$$

where $\lambda = \xi^3/(2k_B T G_0')$ denotes the plasticizing parameter and τ_0 is a ballistic time between monomer collisions, typically of the order of 10^{-13} s.

In order to determine the evolution of free energy barriers during the applied deformation, we need to calculate the dynamics of the average monomer orientation at the scale ξ of dynamical heterogeneities.

II.4. Dynamics of the local tensorial order parameter

The local order parameter $\underset{\sim}{q}$ evolves according to two distinct contributions. The first one is the driving force due to the applied deformation. The local deviatoric stress $\underset{\sim}{\sigma}_{dev}$ induces a tension along each polymer chain. On a given monomer, this tension is given by $\underset{\sim}{\sigma}_{dev} a^2$, where a is one monomer length. This tension is a driving force which progressively orients the monomers. We thus have:

$$a \frac{d\underset{\sim}{q}}{dt} = \frac{\underset{\sim}{\sigma}_{dev} a^2}{2G_0' \tau a} = \frac{\underset{\sim}{\sigma}_{dev} a}{2\eta} \quad (9)$$

where the numerator is the tension and the denominator contains the local viscosity $\eta \approx G_0' \tau$, in which τ is the local relaxation time, which depends on the history of the given subunit and on the local stress, as discussed above and in references.[49,51]

The second contribution makes $\underset{\sim}{q}$ relax to zero in the absence of driving force. The force which restors orientational isotropy is entropic in nature. In order to calculate the

relaxation dynamics, let us consider the orientation vector $\vec{u}$ of a given monomer under an applied tension force $\vec{f}$. The unit vector may be written as $\vec{u} = \vec{u_0} + \delta\vec{u}$, where $\vec{u_0}$ is a fluctuating random vector of average value the nil vector and $\delta\vec{u}$ is a permanent bias due to the applied tension. If $\vec{f}$ is in the i direction, for small δu_i, $\delta u_i \approx af/(3k_BT)$ where $af/(3k_BT)$ is the dimensionless tension.[66] In the absence of this tension and of any other perturbation such as the driving force discussed above, the average orientation vector relaxes on average to the zero tensor. As a consequence, the relaxation of the elongation δu_i is given by

$$a\frac{d\delta u_i}{dt} = -\frac{k_BT}{a\zeta}\frac{af}{k_BT} = \frac{3k_BT}{a\zeta}\delta u_i \tag{10}$$

where $\zeta \sim \eta a \sim G_0'\tau a$ is a friction coefficient at the monomer scale. In terms of the bias vector $\delta\vec{u}$, the order parameter (Equation (5)) can be written

$$q_{i,j} = \frac{1}{2}\langle 3u_iu_j - \delta_{i,j}\rangle = \frac{3}{2}\langle \delta u_i \delta u_j\rangle \tag{11}$$

It follows from equations (10) and (11) that the order parameter $\underset{\sim}{q}$ relaxes to the zero tensor according to this restoring force which derives from the orientational entropy :

$$\frac{dq_{i,j}}{dt} = \frac{3}{2}\left\langle \delta u_i\frac{d\delta u_j}{dt} + \delta u_j\frac{d\delta u_i}{dt}\right\rangle = -\frac{9k_BT}{a^2\zeta}\langle \delta u_i\delta u_j\rangle = -\frac{6k_BT}{a^2\zeta}q_{i,j}$$

or equivalently

$$a\frac{d\underset{\sim}{q}}{dt} = \frac{-6k_BT\underset{\sim}{q}}{a\zeta} = \frac{-6k_BT\underset{\sim}{q}}{G_0'\tau a^2} \tag{12}$$

This equation describes the relaxation of the orientational order parameter by rotational diffusion. In the Supplementary Information document, we consider the orientation relaxation of rigid rods and show that it is essentially equivalent to that given by Equation (12).

Combining Equations (12) and (9), the evolution equation for the local order parameter

is obtained:

$$\frac{d\underset{\sim}{q}}{dt} = \frac{1}{2\tau(\underset{\sim}{q},\underset{\sim}{\varsigma})}\left(\frac{\underset{\sim}{\varsigma}_{dev}}{G'_0} - \frac{12k_BT\underset{\sim}{q}}{G'_0a^3}\right) \tag{13}$$

This equation describes the evolution of $\underset{\sim}{q}$ for each dynamical subunit, considering its own history and relaxation time. Equation (13) is the main physical effect added to the model as compared to references.[48,49,51]

II.5. Effect of the pressure on the dynamics

Equation (8) explicitly incorporates the effect of the deviatoric stress only and not the effect of the hydrostatic component of the stress. Taking the deviatoric stress into account is sufficient when either tensile or compressive tests are considered separately,[50,52,54,67] since the effect of the hydrostatic stress on the relaxation time is relatively small as compared to that of pure shear. On the other hand, this effect must be taken into account when comparing tensile and compressive tests.[5,55] This may be done by adding a multiplicative factor of the form $\exp(a_p^*p)$ to the r.h.s of Equation (8), where $p = -Tr\left(\underset{\sim}{\varsigma}\right)/3$ is the hydrostatic component of the stress (i.e. the pressure) and a_p^* is a constant of the order of 10^{-8} Pa^{-1} typically.[5,57] For the considered experiments, the argument a_p^*p never exceeds a value of the order of 1, whereas relaxation times vary by many orders of magnitude under the effect of the deviatoric component of the stress.[55]

II.6. Discussion

Let us consider the physical meaning of Equations (8) and (13). The discussion here is qualitative and we shed the tensor notation. The ratio $\epsilon = \sigma/G'_0$ between the local stress σ and the glassy modulus G'_0 may be interpreted as a "glassy deformation". Equation (13) then reads

$$\frac{dq}{dt} = \frac{1}{2\tau}\left(\frac{\sigma}{G'_0} - \frac{q}{R}\right) = \frac{1}{2\tau}\left(\epsilon - \frac{q}{R}\right) \tag{14}$$

where $R = G'_0 a^3/12k_BT$. The quantity k_BT/a^3 is the Rouse modulus extrapolated to one monomer. It sets the scale for the orientational entropy forces which restore isotropy through orientational diffusion.[62] The ratio $1/R$ sets the respective effects of the driving force and the restoring force. R is an adjustable parameter of the model. Its approximate value is predicted by the theory. Assuming $a = 0.5$ nm and $T = 290$ K, one has $k_BT/a^3 \approx 3 \cdot 10^7$ Pa, whereas $G'_0 \approx 3 \cdot 10^9$ Pa typically. The ratio R is then between 6 and 10. The relatively large value of R stems from the fact that the Rouse modulus on one monomer scale is smaller by two orders of magnitude than the bulk glassy modulus G'_0.

As a consequence of Equation (14), the local orientational parameter q saturates at a value $q_{max} = R\sigma/G'_0$. Assuming $\sigma = 9 \cdot 10^7$ Pa, $G'_0 = 3 \cdot 10^9$ Pa and $R = 10$, one obtains $q_{max} = 0.3$. q may thus be assumed to remain far below its maximum value 1, which warrants the linear approximation used to derive the dynamical equation (13). Assuming that $\mu_2 \approx 300$, we deduce that an upper bound for the contribution to the local increase of free energy barriers due to monomer orientation is of the order of 30 k_BT_g.

To increase the local order parameter, that is, to rapidly and efficiently orient the monomers, a high local stress value σ is favorable, since both the driving term $\sigma/\tau G'_0$ in Equation (14) and the saturation value $q_{max} = R\sigma/G'_0$ increase as σ increases. As long as the stress has not relaxed yet, the local relaxation time τ is relatively small as a consequence of the decrease of the free energy barriers due to the stress. However, the driving force σ/G'_0 for orienting the monomers is still present. The possible occurrence of strain hardening then results from a fine balance between the increase of free energy barriers due to monomer orientation driven by the stress (Equations (8) and (13)) and the decrease of free energy barriers due to the stress which in turn contributes to shortening the relaxation time τ and accelerate the relaxation of the orientation.

As long as a relaxation event has not taken place yet, the driving force progressively

orients the monomers and the local order parameter increases. Conversely, if a relaxation event takes place, the driving force drops, the relaxation time drops to a low value before increasing again through aging and the local orientation might relax by rotational diffusion.

The parameter μ_2 corresponds to the lowering of interaction energy between perfectly aligned monomers as compared to an isotropic distribution of orientation, and controls the increase of the local free energy barriers and of the local viscosity due to orientation. This effect is due to van der Waals interactions between monomers and is purely enthalpic. The quadrupolar interaction is larger between aligned rods than for perpendicular rods. At low temperature, these interactions (which are essentially independent of temperature) would lead to a nematic state. At temperatures of the order of T_g or above, the equilibrium state is isotropic because the orientational entropy dominates. When monomer orientation is driven in out-of-equilibrium states, this entropy dominates the restoring force, though there are indeed energetic contributions which marginally reduce this restoring force. We only consider the dominant term of orientational entropy as a restoring force, associated to the factor $1/R$.

III. Relaxation mechanisms

We discuss here the 3D numerical implementation which has been developed to solve the theoretical model described above. The numerical model without strain hardening has been described in references.[48,49,51] The local nematic order parameter $\underset{\sim}{q}$ is a new degree of freedom. Dynamical heterogeneities are modeled by both glassy springs characterized by a high frequency elastic modulus G_0' and a local relaxation time $\tau(t_w, \underset{\sim}{\sigma}, \underset{\sim}{q})$ which fluctuates and evolves in time. $\tau(t_w, \underset{\sim}{\sigma}, \underset{\sim}{q})$ depends on the age t_w of the glassy spring, that is the elapsed time since the last breaking event, the local stress $\underset{\sim}{\sigma}$ and the local order parameter $\underset{\sim}{q}$. The strain and stress fields are computed in 3D. The resolution is the size ξ of dynamical heterogeneities. A spatial distribution of relaxation times, which age and relax randomly during

the course of the simulations, is computed and updated at every time step of the simulation.

At each time step dt, a glassy spring relaxes with a probability dP_{rel} given by

$$dP_{rel}(\tau(t_w, \underset{\sim}{\sigma}, \underset{\sim}{q})) = \frac{dt}{\tau(t_w, \underset{\sim}{\sigma}, \underset{\sim}{q})}$$

When a spring relaxes, its age t_w is set to a lower cutoff value t_{min} and the glassy stress is released. Otherwise, the spring ages further by dt. The aging and relaxation processes in glassy polymers in the linear and plastic flow regimes were modeled in this way in references.[48,49,51] According to equation (8), the dependence on $\underset{\sim}{\sigma}$ is introduced by

$$dP_{rel}(t_w, \underset{\sim}{\sigma}, \underset{\sim}{q}) = dP_{rel}(t, 0, 0) \exp\left(\lambda \underset{\sim}{\sigma} : \underset{\sim}{\sigma} - \mu_2 Tr\left(\underset{\sim}{q}^2\right) - a_p^* p\right) \tag{15}$$

where p is the pressure. Assuming $\xi = 3$ nm, $G_0' = 3 \times 10^9$ Pa and $T = 5 \times 10^{-21}$ J, the typical value $\lambda = \xi^3/(2G_0' k_B T) \sim 10^{-3}$ MPa^{-2} is obtained for the plasticizing parameter. This value will be used in our simulations. The deviatoric component σ_{dev} of the stress appears in the argument of the exponential, which becomes of the order of one for a stress of a few tens of MPa's and a strain of a few percents. Regarding the effect of orientation, we have seen that $\mu_2 = \tilde{\mu_2} N_c / k_B T$ may be assumed to be of the order of 300. This value will generally be used in our simulations. Based on experimental data by Govaert et al,[5] we assume that a_p^* is typically of the order of $a_p^* = 10^{-2}$ MPa^{-1}.

The dependence on the age t_w of the glassy spring relaxation rate is given by

$$dP_{rel}(t_w, 0, 0) \simeq -\frac{\mathrm{d} \ln p_{\text{eq}}(\tau)}{\mathrm{d}\tau}\bigg|_{\tau = t_w} dt \tag{16}$$

where $p_{\text{eq}}(\tau)$ is the equilibrium DRT.[48] We assume that the distribution of relaxation times τ_s at equilibrium can be represented by a log-Gaussian probability distribution of central

value $\bar{\tau}$ and width Δ:[16,49]

$$p_{eq}(\mathrm{Log}(\tau_s)) = \frac{1}{\sqrt{\pi}\Delta} \exp(-\frac{\mathrm{Log}^2(\tau_s/\bar{\tau})}{\Delta^2}) \tag{17}$$

with $\mathrm{Log} = \log_{10}$. We further assume that decreasing the temperature slows down the dynamics only by shifting p_{eq} towards longer time scales. The central value $\bar{\tau}$ is computed so that the time τ_{p_c} corresponding to the percolation threshold p_c is equal to τ_α at equilibrium, through the percolation equation :[49,56,68,69]

$$\int_{\mathrm{Log}(\tau_\alpha)}^{\infty} p_{eq}(\mathrm{Log}(\tau_s)) d\mathrm{Log}(\tau_s) = p_c \tag{18}$$

with $p_c \approx 0.11$.

For each dynamical subunit, equations (15) and (16) provide a local relaxation time which depends on its age t_w, is accelerated by the local stress and slowed down by monomer orientation. A "bare" distribution of local relaxation times $Q_\sigma(\tau_s, t)$, from which the long-time cut-off τ_d for α-relaxation is calculated, is obtained in this way. The following expression is then used for the effective relaxation time associated to a subunit of age t_w with a local stress tensor $\underset{\sim}{\sigma}$ and local order parameter $\underset{\sim}{q}$:

$$\tau(t_w, \underset{\sim}{\sigma}, \underset{\sim}{q}, \{\tau_s\}) = \min \left[\tau_s(t_w, \underset{\sim}{\sigma}, \underset{\sim}{q}), \tau_d(\{\tau_s\}) \right] \tag{19}$$

The relaxation probability during dt is given by

$$dP_{rup}(t_w, \underset{\sim}{\sigma}, \underset{\sim}{q}, \{\tau_s\}) = \frac{dt}{\tau(t_w, \underset{\sim}{\sigma}, \underset{\sim}{q}, \{\tau_s\})} = \frac{dt}{\min \left[\tau_s(t_w, \underset{\sim}{\sigma}, \underset{\sim}{q}), \tau_d(\{\tau_s\}) \right]} \tag{20}$$

Equations (15), (16), (19) and (20) altogether contain the effect of aging,[48,49,70] the impact of the stress on the acceleration of the dynamics and the facilitation mechanism (melting of

slow subunits by faster ones).[49,51]

IV. Results and discussion

IV.1. Mechanical properties and strain hardening

Unless otherwise stated, the strain hardening mechanism is implemented in the simulations. All simulations implement the facilitation mechanism: the relaxation time of a given subunit is coupled with the dynamics of neighboring subunits by Equation (19). The reference values for the parameters μ_2 and a_p^* are $\mu_2 = 300$ and $a_p^* = 10^{-2}$ MPa^{-1}. The WLF parameters of polystyrene (PS), with $T_g = 373$ K, have been arbitrarily chosen for this generic description of the model.[14] This choice sets the temperature dependence of the dominant relaxation time of the undeformed polymer in all calculations. Specific polymers and experimental data will be considered in future work. Stress-strain curves obtained with the strain hardening mechanism but without the effect of the pressure ($a_p^* = 0$) are shown in Figures 3.(a) and 3.(b) during tensile and compressive tests, respectively. The true strain ε is defined as $\varepsilon = \ln(L/L_0)$ where L_0 and L are the lengths of the sample in the relaxed and deformed states respectively. No strain hardening is observed at $T = 351$K. The stress-strain curve exhibits a plateau corresponding to a steady state of the relaxation time distribution.[49,51] Strain hardening sets in upon lowering the temperature.

The elastic, yield and stress softening regimes are similar to those obtained in references[49,51] without the strain hardening mechanism. At deformation amplitudes beyond the stress softening regime, a roughly linear increase of the stress with a slope $G_R \sim 10^7 - 10^8$ Pa is observed. The onset of strain hardening occurs at about 15 to 30 % strain amplitude. This behavior is qualitatively consistent with experimental data reported in the literature. G_R vanishes close to T_g and increases as temperature decreases, up to values of about 100 MPa far below T_g. In addition, larger G_R values correspond to smaller stress overshoots during

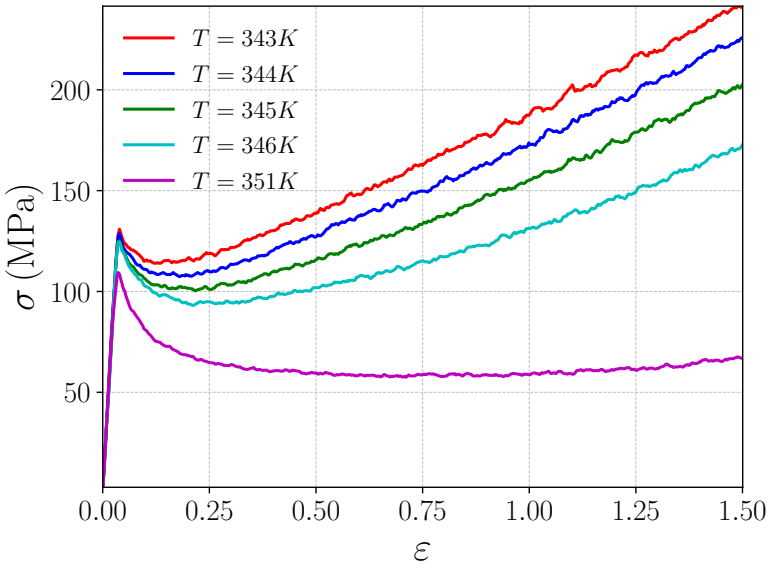

(a)

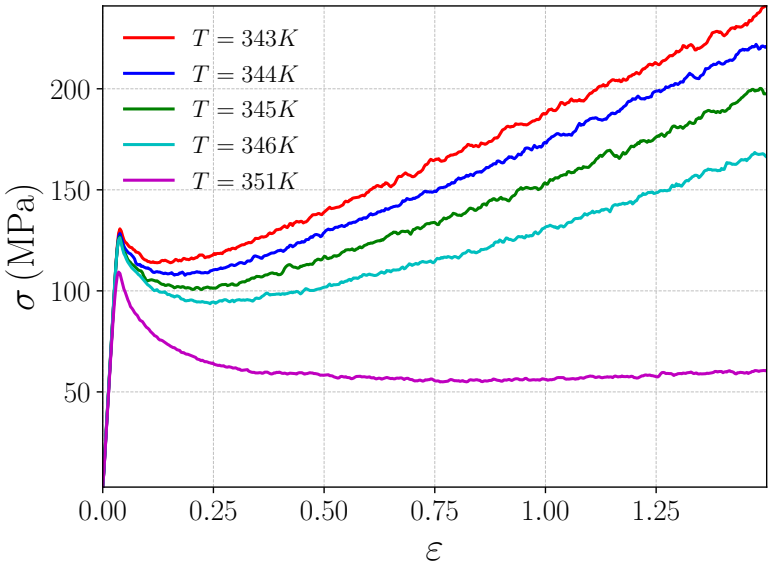

(b)

Figure 3: True stress - true strain curves during uniaxial tensions (a) and uniaxial compressions (b) at different temperatures and at constant true strain rate of 0.1 s^{-1}. The strain hardening mechanism is implemented. The strain hardening parameters are $\mu_2 = 300$ and $a_p^* = 0$ MPa^{-1}. For both tension and compression, no strain hardening is present at $T = 351$ K whereas strain hardening sets in at lower temperatures. The lower the temperature, the higher the strain hardening modulus. Note that as the effect of pressure is not taken into account, the mechanical responses in both tension and compression are similar.

stress softening, which is also observed in experiments.[7] Note that, as the specific contribution of the pressure is not taken into account, both series of curves in Figures 3.(a) and 3.(b) are very similar.

We describe the α-relaxation as a random process. When a relaxation event takes place, the stress is entirely relaxed, the dynamics of the subunit becomes fast and starts aging again. As a result, the stress-softening is somewhat sharper than that observed experimentally. Our point of view is that comparing in detail results of our simulations to experimental data in this regime could give important clues regarding the physics of the α-relaxation and the facilitation mechanism itself and may allow to describe a more progressive relaxation with more details as regards to the physics involved. The key for a better description of the stress softening would be a finer description of the α-relaxation and of the facilitation mechanism themselves.

Stress-strain curves obtained at different temperatures and different strain rates are plotted in Figure 4.(a) and Figure 4.(b) respectively, for both tension and compression tests. The lower the temperature or the higher the strain rate, the higher the strain hardening modulus for both tension and compression. Note that the higher temperature in Figure 4.(a) and lower strain rate in Figure 4.(b) both nearly correspond to the onset of the strain hardening. For the same temperature and strain rate, the stress level in compression is systematically larger than in tension. In our model, this difference is entirely due to the effect of the pressure. Simulations of tensile and compressive tests with various values of the pressure parameter a_p^* have been performed at 345 K and strain rate of 0.1 s^{-1}. The obtained stress-strain curves are shown in Figure 5. The larger the value of a_p^*, the larger the difference between tension and compression. Note that the curves are much less noisy than those in reference,[49] as the size of the simulation box is 4 times larger and the time step 10 times shorter than in.[49]

As shown in Figure 4.(b), the strain hardening increases as the strain rate increases. In fact, as the strain rate increases, the stress increases over the whole range of deformation,

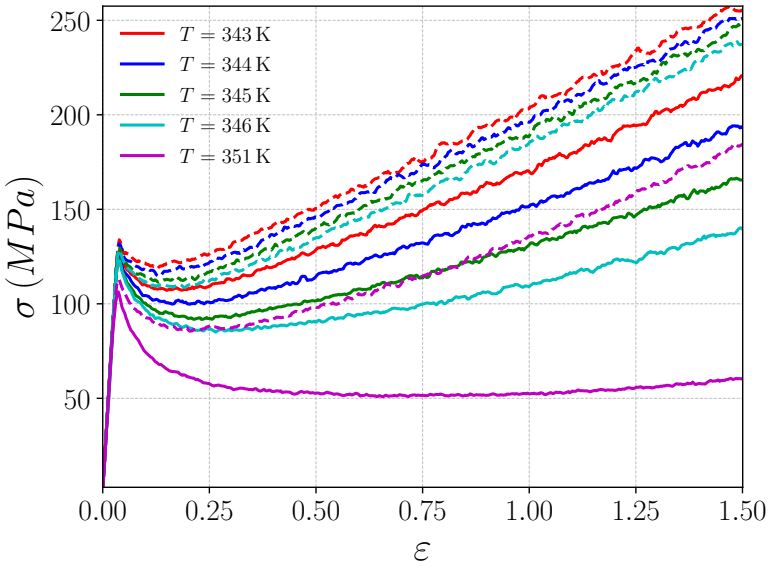

(a)

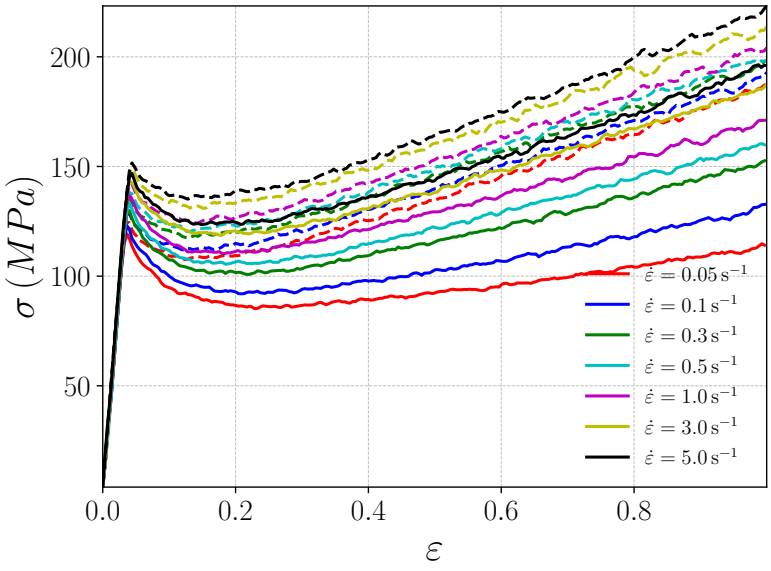

(b)

Figure 4: True stress-true strain curves during uniaxial tensions (full curves) and compressions (dashed curves): (a) at different temperatures and at constant true strain rate 0.1 s^{-1}, and (b) at different strain rates at a constant temperature 345K. The strain hardening mechanism is implemented with parameters $\mu_2 = 300$ and $a_p^* = 0.01$ MPa^{-1}. At the lower strain rate, the strain hardening regime is barely present. The higher the strain rate, the higher the strain hardening modulus. Note that compressive stress-strain curves exhibit systematically stronger strain hardening than do tensile curves due to the effect of pressure.

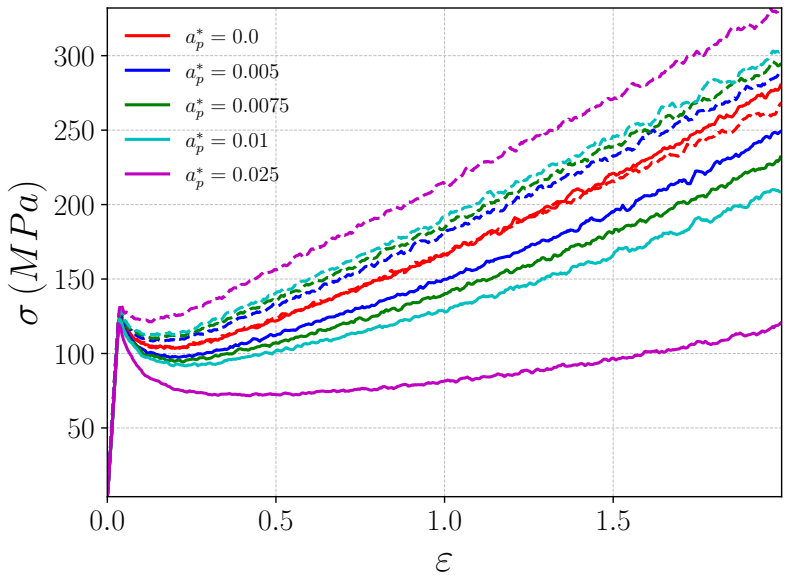

Figure 5: True stress - true strain curves during uniaxial tensions (continuous curves) and compressions (dashed curves) for different values of a_p^* in MPa^{-1}. Simulations are performed at a constant temperature 345K and constant true strain rate 0.1 s^{-1}. The strain hardening mechanism is implemented. The strain hardening parameter is $\mu_2 = 300$. Compressive stress-strain curves exhibit a stronger strain hardening behavior than tensile ones due to the effect of pressure.

which is consistent with experimental results.[71]

The modulus G_R is roughly proportional to the logarithm of the strain rate. G_R is plotted as a function of temperature in Figure 6, for simulations run at a constant strain rate $0.1\,\mathrm{s}^{-1}$. G_R decreases and strain hardening is less pronounced as temperature increases. G_R vanishes at about $T = 352\mathrm{K}$, that is $T \approx T_g - 21\mathrm{K}$.

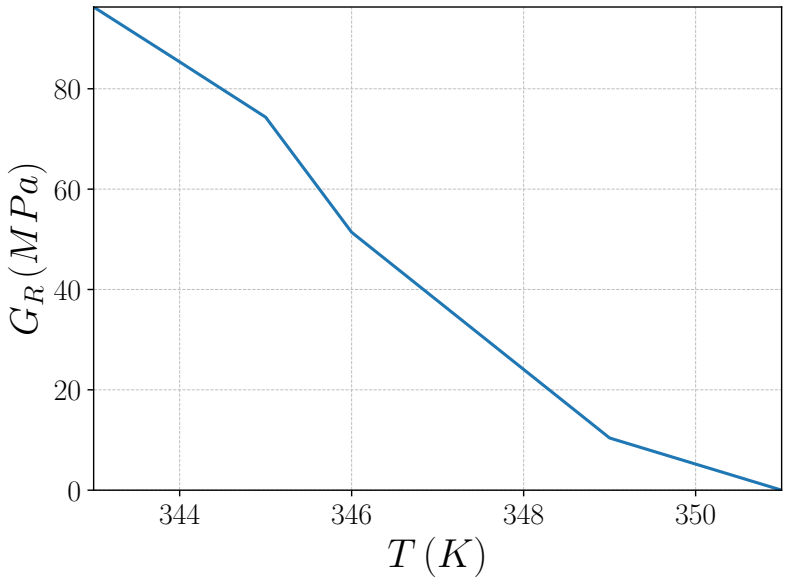

Figure 6: Evolution of the hardening modulus G_R as a function of temperature during tensile tests performed at $-0.1\,\mathrm{s}^{-1}$. The strain hardening parameters are $\mu_2 = 300$ and $a_p^* = 0$ MPa^{-1}.

IV.2. Orientation

The evolution of the average value of the order parameter $Tr\left(\underset{\sim}{q}^2\right)$ as a function of the strain is shown in Figure 7, for different temperatures. Not far below T_g, the order parameter does not increase significantly under deformation, because the monomer orientation relaxes too fast. As temperature decreases below $T_g - 25$ K, the average $Tr\left(\underset{\sim}{q}^2\right)$ value increases up to about $6 - 7$ % at large deformation. At small strain, monomer orientation is too small to induce a significant increase of free energy barriers for α-relaxation. As a consequence, the yield stress and the stress softening regime are not significantly modified, even though the

yield stress is slightly increased and stress softening slightly reduced in the presence of the strain hardening mechanism.

The observed average $Tr\left(\underset{\sim}{q}^2\right)$ value at deformation $\varepsilon \sim 1$ at the lowest considered temperatures is about 3×10^{-2}. This value leads to an average increase of free energy barriers due to monomer orientation of the order of $9k_BT_g$, which is quite large. However, we shall see later that the increase of $Tr\left(\underset{\sim}{q}^2\right)$ is strongly heterogeneous and that the effect observed on stress-strain curves cannot be understood by considering the average $Tr\left(\underset{\sim}{q}^2\right)$ value only. The average value of $S = | < q_{33} > |$ is plotted in Figure 8, for both tension

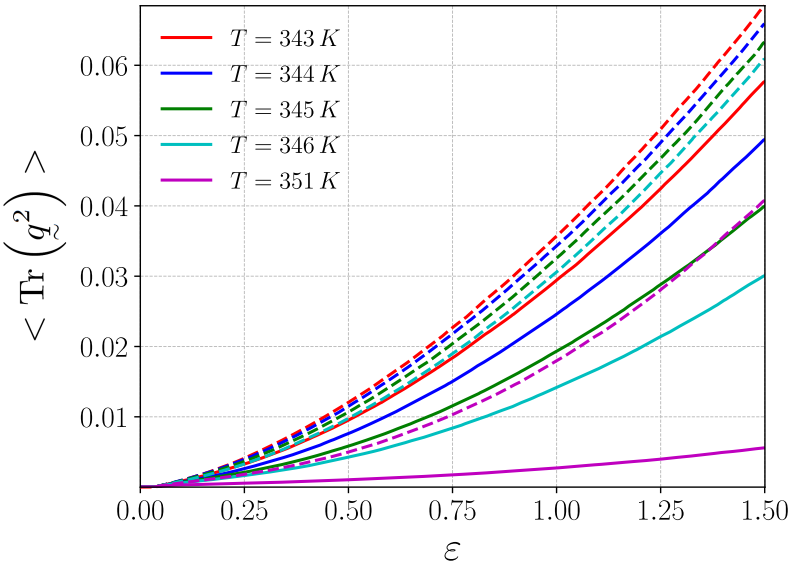

Figure 7: Average orientational parameter $< \mathrm{Tr}\left(\underset{\sim}{q}^2\right) >$ as a function of true strain during uniaxial tensions (continuous lines) and uniaxial compressions (dashed lines) at a constant true strain rate $\dot{\varepsilon} = 0.1\ \mathrm{s}^{-1}$. The different colors correspond to different temperatures. Highest orientation is observed at low temperatures, due to the reduced mobility and higher stress levels. The strain hardening parameters are $\mu_2 = 300$ and $a_p^* = 0.01\ \mathrm{MPa}^{-1}$.

and compression tests along direction 3. At the lowest considered temperatures and at large deformations, S takes values of the order of 0.1-0.15, comparable to the values measured by NMR by Vogt et al in polycarbonate.[72] Figure 8 also shows that the orientation does not increase significantly for the highest considered temperature. This temperature of about $T_g - 21\mathrm{K}$ corresponds to the temperature at which the modulus G_R vanishes. Note that

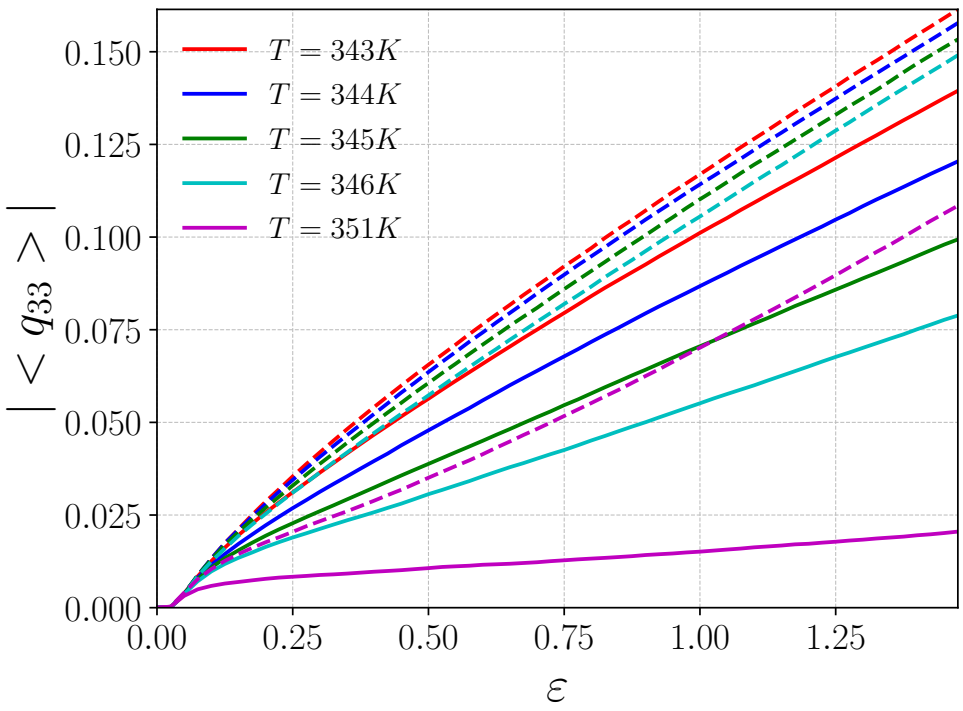

Figure 8: Evolution of $S = |< q_{33} >|$ as a function of true strain during uniaxial tensions (continuous lines) and uniaxial compressions (dashed lines) at a constant strain rate $\dot{\varepsilon} = 0.1$ s^{-1} along direction 3. The different colors correspond to different temperatures. The strain hardening parameters are $\mu_2 = 300$ and $a_p^* = 0.01$ MPa^{-1}.

$< Tr\left(\underset{\sim}{q}^2\right) >$ and $S = |< q_{33} >|$ are quadratic and linear functions of the order parameter respectively, hence the different variations in Figures 7 and 8.

IV.3. Evolution of the free energy barriers

The cumulative distributions of orientation $F\left(\mathrm{Tr}\left(\underset{\sim}{q}^2\right)\right)$, of elastic energies $F\left(\lambda\,\underset{\sim}{\sigma} : \underset{\sim}{\sigma}\right)$ and of the entire barrier modifications for α-relaxation $F\left(\{-h_{tot}\}\right)$ where $-h_{tot} = \lambda\,\underset{\sim}{\sigma}:\underset{\sim}{\sigma} - \mu_2 \mathrm{Tr}\left(\underset{\sim}{q}^2\right)$ are plotted at different strain values in Figures 9.(a), 9.(b) and 9.(c), respectively. The cumulative distribution F of a positive random variable x is defined by $F(x) = \int_0^x p(u)\,\mathrm{d}u$, where p is the distribution function of the variable. By definition $F(x \to +\infty) = 1$.

The evolution of the distribution of $\mathrm{Tr}\left(\underset{\sim}{q}^2\right)$ (Figure 9.(a)) is monotonic, with an overall shift towards higher values as ε increases (see also Figure 7). Conversely, the evolution of

the distribution of $\lambda_{\underline{\underline{\sigma}}} : \underline{\underline{\sigma}}$ (Figure 9.(b)) is not monotonic. Up to yield ($\varepsilon \approx 4$ %) and during stress softening (up to about 25 % true strain), the evolution of elastic energies is the same as the one without the strain hardening mechanism. The elastic energies decrease during stress softening. Then, in the strain hardening regime, instead of remaining stationary, the distribution of elastic energies shifts towards higher values again.

Figure 9.(c) shows that at small strain values, energy barriers for α-relaxation always decrease (i.e. shift towards the right-hand side of the graph). However, when subunits start to get oriented (at approximately 25 % true strain), some energy barriers increase (shift towards the left-hand side of the graph). At strain values as high as 75 % and 150 %, a significant fraction of subunits have very high energy barriers. Even though such high barriers (of the order of 50 $k_B T_g$) should correspond to inaccessibly long relaxation times, the corresponding subunits may relax with a characteristic time τ_d as a consequence of the facilitation mechanism (see also Figure 12). Since some subunits have high elastic energy levels and contribute to a large decrease of free energy barriers, we deduce that the orientation and stress are correlated: subunits which bear a large stress are also strongly oriented, as could be expected.

A fraction of subunits which bear no stress and are oriented may exist as a consequence of the difference between the relaxation rate of the stress, which may be fast, and that of orientation, which is progressive. Consider a particular subunit which has stored a high local stress, that is a high local elastic energy, and which in turn has oriented significantly. When this subunit undergoes a relaxation event at $t = 0$, the local stress (the driving force for orientation in equation (13)) drops instantly to zero, while the local orientation remains unchanged at $t = 0^+$ and relaxes progressively under the effect of the entropic relaxation force in equation (13). It results that the energy barrier of this subunit suddenly increases by a large amount (roughly corresponding to the elastic energy stored by the subunit before the relaxation event) and subsequently decreases progressively as local orientation relaxes.

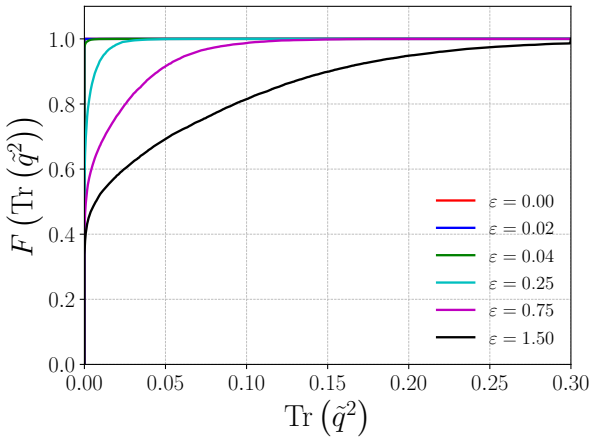

(a)

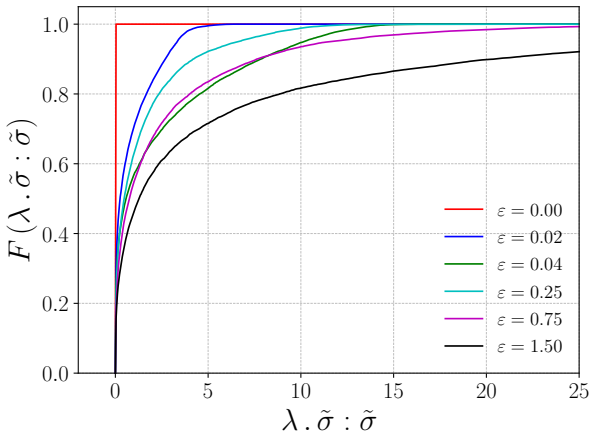

(b)

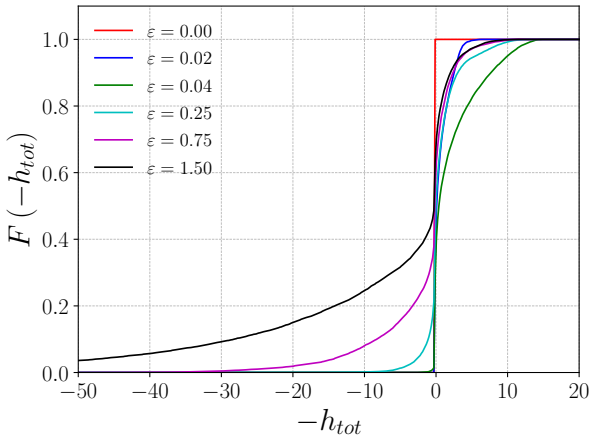

(c)

Figure 9: Cumulative distribution functions computed at different true strain values, during a tensile test at 345 K and 0.1 s^{-1}, for: (a) the orientations $\mathrm{Tr}\left(\underset{\sim}{q}^2\right)$; (b) the elastic energies; (c) the entire free energy barrier modification for α-relaxation (multiplied by -1) at the scale of subunits. The strain hardening mechanism is implemented, with strain hardening parameters $\mu_2 = 300$ and $a_p^* = 0$ MPa^{-1}. Abscissa scales are in units of k_BT.

IV.5. Influence of model parameters

The main adjustable parameters of the model are λ, μ_2 and R. λ, which is the key parameter for yield stress, is directly related to the dominant scale ξ of the α-relaxation process. The value of this length ξ is approximately, but not exactly, known. μ_2, which sets the increase of free energy barriers as a function of monomer orientation, is related to the anisotropy of the monomer polarizability, to the Kuhn length and to the scale ξ. Note that in non-polar polymers, that is polymers with no permanent dipoles, monomer interactions are mostly van der Waals interactions, which are essentially dipolar interactions between fluctuating and induced dipoles. This interaction between monomer A and monomer B involves the product of the electron polarizabilities of these monomers, $W \sim p_A p_B$, which are most frequently larger for parallel monomers than for perpendicular ones.[63,73] The order of magnitude of μ_2 is about 300, but its precise value depends on those polymer details. The order of magnitude of $1/R$, which sets the relaxation rate of monomer orientation in the absence of driving force, is predicted by the theory to be of the order of 0.1. We consider here how strain hardening depends on the precise values of these adjustable parameters.

Stress-strain curves are plotted for different values of the parameter λ in Figure 10.(a). When λ decreases, both the yield stress σ_y and post-yield stress values increase. Strain hardening is also more pronounced, with a larger hardening modulus. This is due to the fact that smaller values of λ lead to smaller decrease of the free energy barriers as a function of the stress, and thus to longer relaxation times at a given stress level. Orientation is enhanced as a consequence of the slower relaxation of the orientation. Conversely, strain hardening is less pronounced upon increasing λ and becomes small, with stress values always smaller than σ_y even in the strain hardening regime, for values of λ larger than $1.5 \times 10^{-3}\mathrm{MPa}^{-2}$.

Tensile stress-strain curves obtained for different values of μ_2 are plotted in Figure 10.(b).

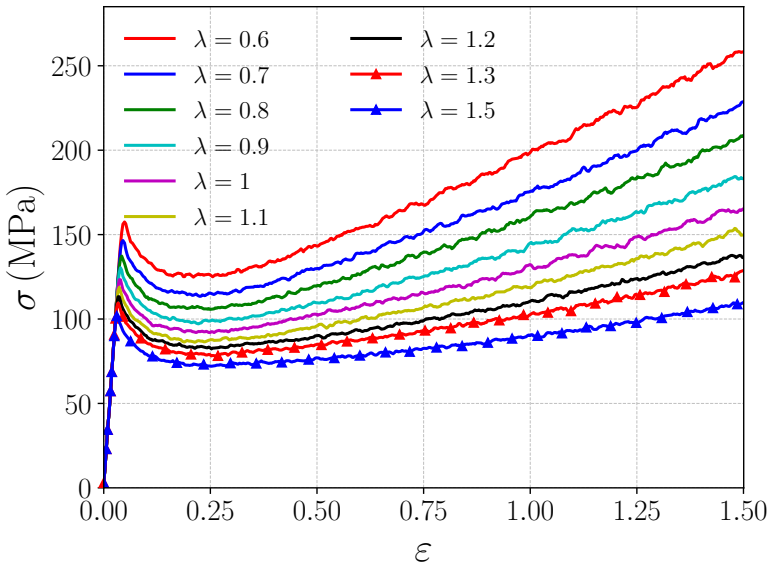

(a)

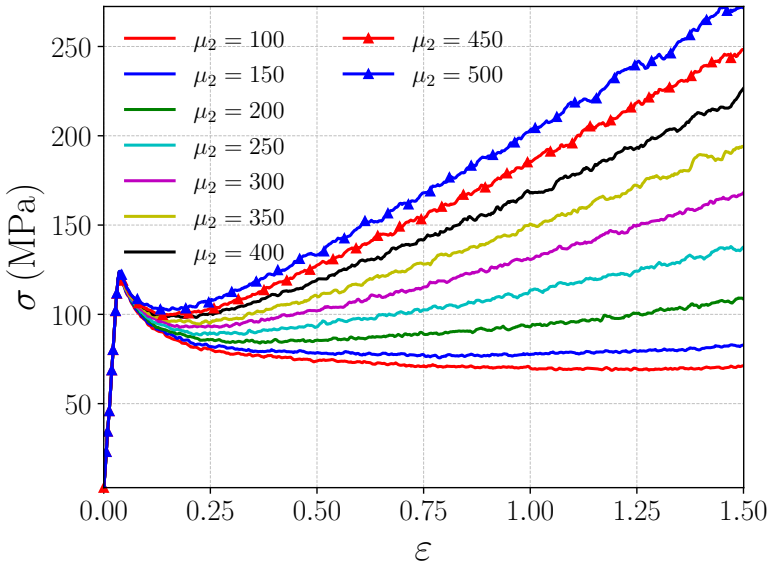

(b)

Figure 10: Stress-strain curves during tensile tests at 345 K and 0.1 s^{-1}: (a) for different values of λ. Indicated λ values are in units of $10^{-3}\,\mathrm{MPa}^{-2}$. Other parameter values are $\mu_2 = 300$, $a_p^* = 0.01$ and $1/R = 0.1$; (b) for different values of μ_2. Other parameters values are $\lambda = 10^{-3}\,\mathrm{MPa}^{-2}$, $a_p^* = 0.01$ and $1/R = 0.1$.

It appears that μ_2 has no influence on the elastic regime nor on yield because monomer orientation is negligible at small deformation. However, the stress values during stress softening and strain hardening, as well as the hardening modulus, are strongly affected by μ_2. The higher μ_2, the higher the stress values after yield and the more pronounced the strain hardening. In particular, a strong strain hardening is observed for values of μ_2 larger than typically 400. Higher values of μ_2 lead to a more rapid increase of free energy barriers, and thus a more pronounced slowing down of the dynamics, upon deformation. Furthermore, higher stress values also mean a stronger driving force for orientation, which is thus enhanced.

Conversely, strain hardening altogether disappears for values of μ_2 smaller than 200: below a critical value for μ_2, monomer orientation does not allow free energy barriers to increase enough to overcome the reduction of barriers due to the stress.

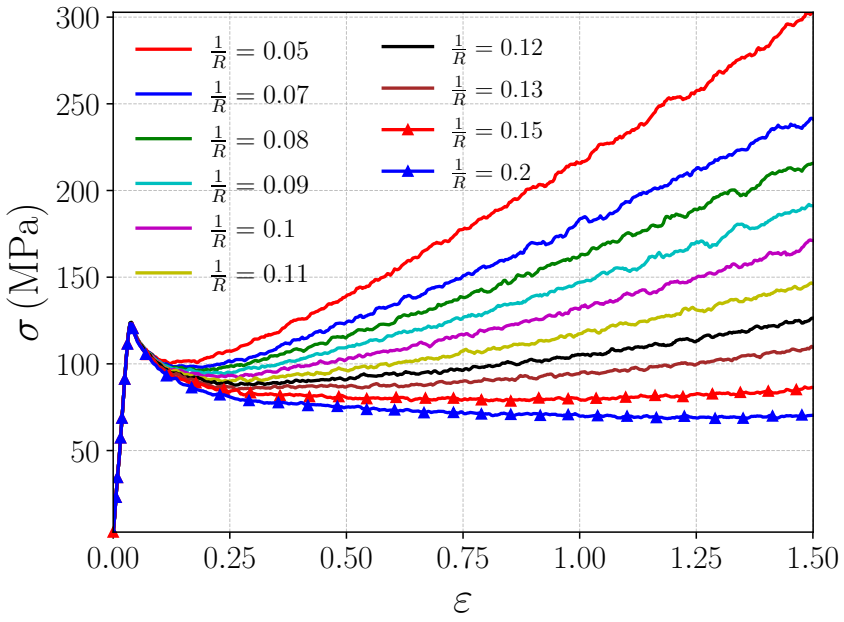

Figure 11: Stress-strain curves during tensile tests at 345 K and 0.1 s^{-1} for different values of $\frac{1}{R}$. Other parameter values are $\lambda = 10^{-3}\,\mathrm{MPa}^{-2}$, $\mu_2 = 300$ and $a_p^* = 0.01$.

The last key parameter for the theory of strain hardening is the relaxation rate of monomer orientation, which is controlled by the parameter $1/R \sim 0.1$. Stress-strain curves

are plotted for different values of $1/R$ in Figure 11. Strain hardening is more pronounced for smaller values of $1/R$, that is when monomer orientation relaxes more slowly. Monomers then get more oriented and free energy barriers increase faster. Conversely, strain hardening is less pronounced for larger values of $1/R$. Typically, strain hardening is strong for $1/R = 0.05$ and vanishes for $1/R = 0.2$. Note that the critical values of the model parameters considered in this discussion are inter-dependent.

Note that the local orientation is calculated based on the assumption of affine deformation on all scales and on Rouse-like relaxation on the monomer scale. We do not consider relaxation modes on larger scales. These modes of course have a slower relaxation than those at the monomer scale, but the corresponding orientation is also smaller and contributes less to the enhancement of free energy barriers. In the Rouse model, the modes are not coupled and each mode relaxes to zero irrespective of the other modes. For long chains, one should in principle introduce a coupling between local orientation and larger scale orientation, as it is considered in the reptation model. On the other hand, the intermediate orientation due to this coupling would be small. Whatsoever, in the strain hardening regime, the relaxation on the monomer scale is already much slower than the time scale of the applied strain due to the the large value of the parameter $R \sim 10$. This is the reason why we consider that the orientation dynamics on the scale of one monomer is the dominant contribution to strain hardening. Future extension of the theory may implement Rouse-like relaxation modes on larger scales and reptation-like orientation.

V. Relaxation times

V.1. Distribution of relaxation times

The DRTs are displayed in figure 12 for various strain values during a tensile test at 345 K and 0.1 s^{-1}. The strain hardening mechanism is implemented. Up to the end of stress

softening (about 25 % true strain), they are quite similar to the ones obtained without the strain hardening mechanism (see Figures 7 and 8 in reference[51]). The initial distribution (corresponding to the initial glassy state) is progressively erased and a new contribution at shorter times emerges (the peak on the left hand-side of the distribution). As the stress starts to increase at larger strain values, this latter part of the distribution shifts towards longer times. This shift does not occur when the strain hardening mechanism is not implemented. Equivalently, the fraction of subunits with long relaxation times increases at large strain values. These subunits with increasingly long relaxation times either have never relaxed and go on aging during deformation, or their local order parameter S has increased significantly under strain. The fraction of fast subunits is smaller and smaller as the strain increases in the strain hardening regime, as a consequence of an enhanced on-going aging process resulting from the increase of the free energy barriers for α-relaxation. Even relatively fast subunits also get oriented, which slows down not only their local dynamics, but also the global dynamics through an increase of τ_d. As a consequence, the relaxation by the facilitation mechanism is slowed down. For each distribution of relaxation times, the long-time cut-off τ_d resulting from the facilitation mechanism is indicated by a vertical dashed line in Figure 12. It is observed that τ_d first decreases as deformation increases up to the onset of strain hardening, at about $\epsilon \sim 0.25$. Then, τ_d starts increasing during strain hardening, that is for ϵ values larger than or equal to about 0.25. Note that τ_d is constant during plastic flow when the strain hardening mechanism is not implemented.[51]

V.2. Evolution of relaxation times

There are several ways to define the dominant relaxation time in the presence of a broad DRT covering many decades. Physically, the dominant relaxation time of the system is assumed to be $\tau_\alpha = \min\{\tau_d, \tau_{pc}\}$.[14,56,58,69] At equilibrium, both τ_d and τ_{pc} are equal.[14,58] During aging after a downwards temperature jump, τ_d becomes larger than τ_{pc} and τ_α is equal to τ_{pc}. Upon rejuvenating by heating, τ_d becomes smaller than τ_{pc} and τ_α is equal to

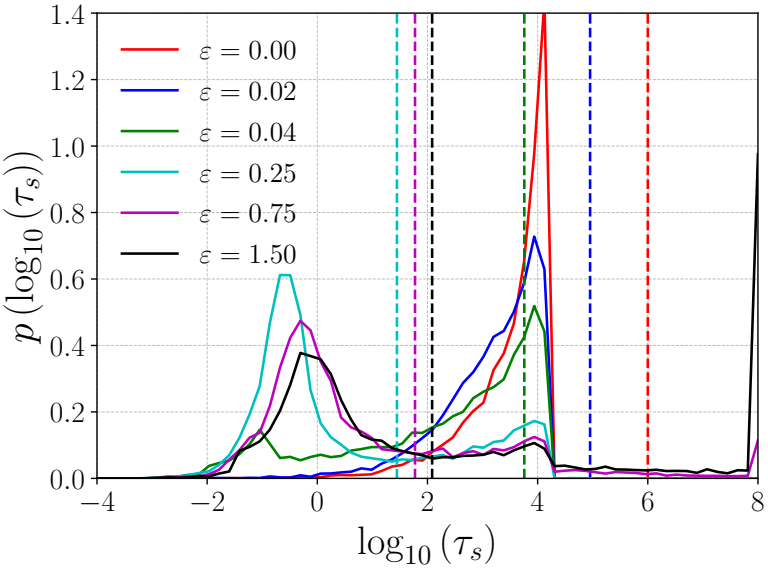

(a)

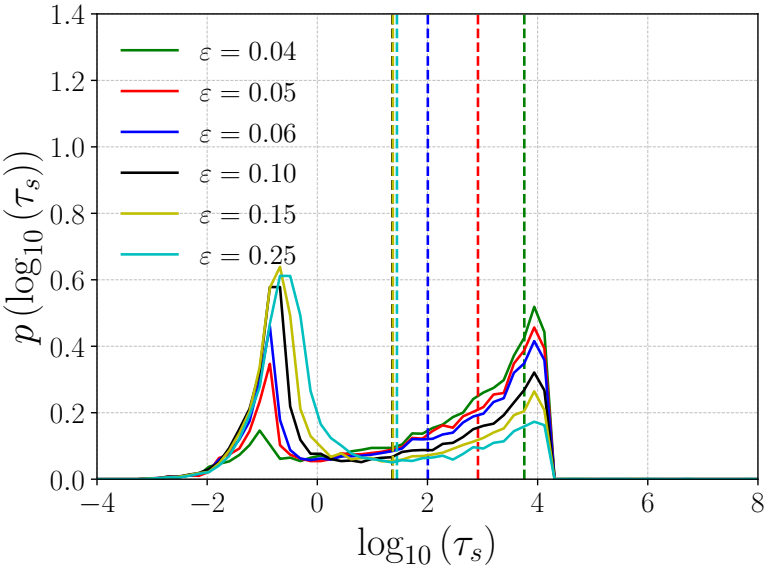

(b)

Figure 12: Distributions of relaxation times during a uniaxial tension at 345 K and at constant true strain rate of 0.1 s^{-1}, with strain hardening parameters $\mu_2 = 300$ and $a_p^* = 0$ MPa^{-1}. Dashed vertical lines indicate the values of τ_d at the indicated true strain values. The deformation amplitudes vary from 0 to 1.5. We display the distribution on two different sub-figures for the sake of clarity.

τ_d. A similar situation takes place when deforming a glassy polymer: τ_d becomes smaller than τ_{pc} and slow subunits are melted by faster ones (facilitation mechanism) so that $\tau_\alpha = \tau_d$. This process is responsible for the narrowing of the distribution of relaxation times during early stages of plastic deformation, before strain hardening takes place.[51] In our simulations, stress relaxation is solved numerically and the dominant relaxation time is the result of the 3D calculation.

Another way to measure a dominant relaxation time experimentally is to integrate the relaxation function, which provides a dominant relaxation time τ_c. This has been commonly done *e.g.* in the group of Ediger with the orientation funcrtion of fluorescent probes.[25] The same can be done in our numerical simulations by calculating the relaxation function $F(t,t_w) = \int_0^{+\infty} \exp(-t/\tau) P(\tau,t_w) d\tau$ where $P(\tau,t_w)$ is the DRT at time t_w.[49,51] Fitting $F(t,t_w)$ with a stretched exponential then gives the Kohlrausch exponent β and an average correlation time τ_c. Those three quantities τ_d, τ_{pc} and τ_c have been found to be consistent with each other.[49,51] We can thus compare the evolutions of τ_d or τ_c and β in our simulations to those of τ_α and β in experiments, such as those measured by Sahli et al,[26] Hem et al[27,28] and Lee et al.[18–20]

We first consider the evolution of the relaxation time τ_d. The evolutions of both the stress and τ_d as a function of strain are plotted in the same graph in figure 13 for a tensile test at 345 K and 0.1 s^{-1}, with strain hardening parameters $\mu_2 = 300$ and $a_p^* = 0$ MPa^{-1} (the results with $a_p^* = 0.01$ MPa^{-1} being similar).

In the simulations, the initial relaxation time τ_d, corresponding to an aged glassy polymer, is larger than 10^5 s. τ_d first decreases upon deformation as some elastic energy is stored and induces an acceleration of the dynamics. At yield, τ_d still has a relatively large value of about 3×10^3 s. Upon increasing the strain further, τ_d goes on decreasing beyond yield until it reaches a minimum during stress softening, at about 6-7 % strain. Then it remains fairly constant for a few additional per cents of strain and starts to increase before the onset of strain hardening. The fact that τ_d increases before strain hardening starts is due to the

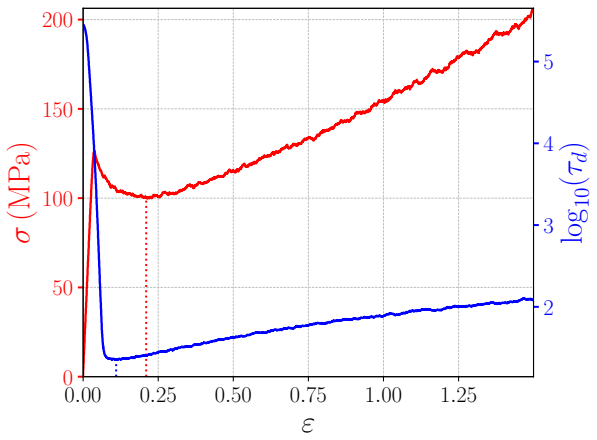

(a)

Figure 13: Evolutions of both the true stress and τ_d as a function of the true strain shown on the same graph during a uniaxial tension at 345 K and at 0.1 s^{-1}. Strain hardening parameters are $\mu_2 = 300$ and $a_p^* = 0\text{MPa}^{-1}$. The true strain goes up to 1.5. The minimum of the stress and of the relaxation time τ_d are indicated by dotted line. The latter starts increasing before the stress increases.

stress softening, as free energy barriers increase when σ relaxes. During strain hardening, the stress increases with a nearly constant slope, and so does τ_d. The evolution of τ_d is quite similar to the experimental evolution of the dominant relaxation time.[27]

The evolutions of τ_d during mechanical tests performed at $0.1\,s^{-1}$ and at different temperatures are plotted in figures 14.(a) and 14.(b). In Figure 14.(a), the strain hardening mechanism is not implemented and τ_d remains constant at large deformations. In Figure 14.(b), the strain hardening mechanism is implemented, and τ_d increases in the strain hardening regime (see also Figure 12).

Let us consider now the evolutions of the Kohlrausch parameter β and of the average correlation time τ_c obtained by fitting the relaxation functions of the stress with a stretched exponential $\exp(-(t/\tau_c)^\beta)$, as a function of the deformation. The results are shown in figure 15 at 3 different temperatures (343 K, 344 K and 345 K). At the 3 temperatures, the evolution of τ_c (Figure 15a) are identical up to the very beginning of stress softening, at about

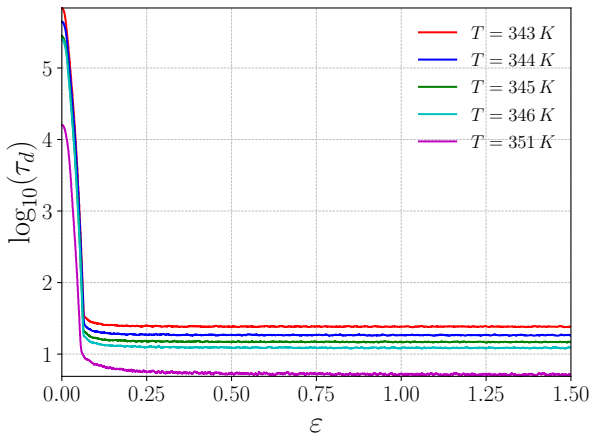

(a)

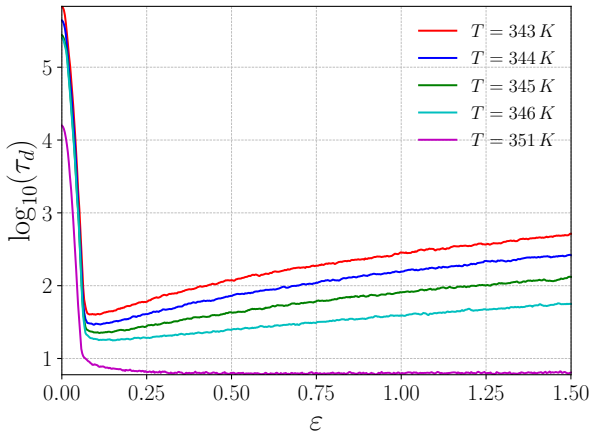

(b)

Figure 14: Evolution of τ_d during uniaxial tensions at different temperatures and at constant strain rate 0.1 s^{-1}, (a) without strain hardening ($\mu_2 = 0$ and $a_p^* = 0$), and (b) with strain hardening ($\mu_2 = 300$ and $a_p^* = 0$).

8 % true strain. Beyond this point, the curves are different: the lower the temperature, the higher the value of τ_c and the sooner it starts increasing again in the strain hardening regime. The evolution of τ_c is very similar to that of τ_d or τ_α at the same temperatures. The evolution of β (Figure 15b) is non-monotonic, as has been observed experimentally by the groups of Ediger[18–20] and of Ciliberto.[26–28] In the same way as in simulations without strain hardening, β first increases up to a temperature dependent strain value of about 30 to 45 %, which corresponds to the onset of strain hardening. This increase of β corresponds to a decrease of the width of the DRT. Then β decreases up to the end of the tensile test, which corresponds to an increase of the width of the DRT during strain hardening, as observed experimentally by Lee et al[18–20] and by Hem et al.[27,28]

The narrowing of the DRT up to and slightly beyond the stress softening regime may be interpreted as follows. Fast dynamical subunits relax very frequently and cannot store elastic energy. Their relaxations times are little affected by the applied strain. The majority fraction of subunits, which have intermediate relaxation times, both sustain the stress and relax. They are accelerated because free energy barriers are lowered by the stress. This process contributes to shift part of the DRT towards shorter times. Conversely, very slow subunits would not relax if they would persist in their slow state, which would result in a broadening of the DRT. However, as the intermediate part of the distribution shifts towards shorter times, the melting time τ_d decreases. As a consequence, slower subunits melt on a time scale shorter than at equilibrium, due to the enhanced Merabia-Long facilitation mechanism.[14,45,51,58]

If the fraction of subunits with increased free energy barriers is large enough, τ_d increases and aging takes place during stretching. Relaxation events are less frequent and the stress gets higher. The increase of free energy barriers, particularly that of subunits with intermediate relaxation times which are less prone to relax and thus more prone to get oriented than

faster ones, makes the facilitation process less efficient. The slowest part of the relaxation times spectrum goes on aging, whereas fast subunits remain fast. As a consequence, the width of the DRT increases during strain hardening, as observed in Figure 15. Up to stress softening, at about 15 % true strain, the evolution of β does not depend on temperature. Beyond this point, the curves start to differ : the lower the temperature, the more efficient the monomer orientation process, the earlier the strain hardening and the decrease of β due to the enhanced aging process. The evolution of β is quantitatively consistent with recent experimental results by Hem et al[27,28] and qualitatively consistent with earlier experimental results by Lee et al.[18–20] The evolution of τ_c is also consistent with recent experimental data.[26,27]

VI. Discussion and Conclusion: physical origin of strain hardening

In our microscopic description of the strain hardening mechanisms, the change of free energy barriers due to the applied strain is the sum of two terms. The first term reduces the barriers and scales like the square of the deviatoric part of the stress. Consistently with the model proposed by Chen and Schweizer,[46] we introduce a second term which increases the barriers and scales like the square of a nematic-like tensorial order parameter describing monomer orientation. The first term relaxes immediately as a function of the applied stress whereas, deep in the glassy state, the second one relaxes very slowly. The dynamics of monomer orientation in glassy polymers submitted to an applied strain is explicitly computed.

Based on this model and on the results presented above, the physical origin of strain hardening may be interpreted as follows. Below the onset of stress softening, monomer orientation is negligible and energy barriers for α-relaxation decrease due to the stored elastic energy. Would there be no orientation, beyond the stress softening regime, the elastic

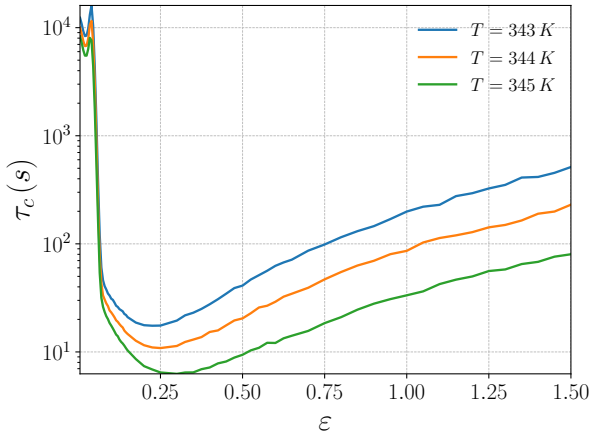

(a)

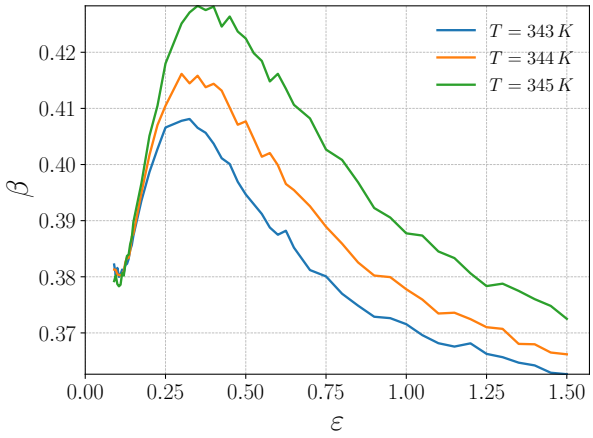

(b)

Figure 15: (a): Evolution of the average correlation time τ_c (a) and of the Kohlrausch parameter β (b) obtained by fitting the relaxation function $F(t)$ with a stretched exponential function during tensile tests performed at 3 different temperatures (343, 344 and 345 K) and at a constant strain rate 0.1 s^{-1}. The strain hardening mechanism is implemented, with strain hardening parameters $\mu_2 = 300$ and $a_p^* = 0$.

energy distribution would reach a steady state leading to stationary plastic flow at constant stress. However, on deforming beyond the onset of stress softening, monomer orientation increases and start contributing to increase the local free energy barriers for α-relaxation. At some point, this effect eventually overcompensate the decrease of the free energy barriers due to the local stress. Relaxation times then start increasing and strain hardening sets in.

The non-monotonic evolutions of the α-relaxation time and of the width of the DRT are also explained by the model. The decrease of the width of the DRT up to stress softening is a consequence of the facilitation mechanism, which is at the very heart of the α-relaxation process.[14,58] The strain hardening regime is the result of a positive feedback. Monomer orientation increases the free energy barriers and thus the subunit relaxation times, which in turn further favors increasing orientation. The facilitation time τ_d, which is the effective subunit relaxation time, increases as a consequence of the overall shift of the DRT towards longer time-scales. The increase of the width of the DRT at large deformations is the result of the enhancement of aging due to the increase of free energy barriers.

The studied temperature range is comprised between $T_g + 50$ K and $T_g - 30$ K (420 K - 343 K), with a particular focus on the temperature range where strain hardening sets in and becomes strong, that is between 352 K and 343 K. Results at higher temperature display a plastic flow at constant stress level and no yield stress at all above T_g. This narrow range is related to the specifically chosen WLF law (displayed in reference 49), which is quite sharp below T_g. The equilibrium relaxation time increases from 10^4s up to about 10^6s between 352 K and 343 K. For the lowest considered temperatures, the samples do not reach equilibrium, as it is frequently the case in experiments. In its current state, the theory would predict quite similar strain hardening at lower temperatures, because what matters most is the dynamical state of the samples which are in any case limited by their age, that cannot be longer than the aging time 10^5s. Upon aging further, we may expect stronger strain hardening on theoretical grounds. The current version of the numerical model is stable down

to temperatures close to $T_g - 30$ K (340 K) and becomes unstable at lower temperatures, where the current distributions of relaxation times are too far from the equilibrium one. Solving the numerical model at temperatures lower than $T_g - 35$ K would require extension of the numerical tool we have developed.

However, one should keep in mind that the physics of aging itself becomes more complex at lower temperatures and cannot be described by such simple aging dynamics as that of Merabia and Long.[58,74] For instance, polycarbonate does not age at room temperature and ages more rapidly at T_g-20 - T_g-30 K because the dynamics is not frozen in that temperature range. In reference,[28] we interpreted this fact as a consequence of the dependence of the relaxation times on both the density and temperature. If temperature is too low, aging is frozen. On the other hand, aging takes place even at room temperatures under stress as the dynamics is accelerated due to the stress.

At even lower temperatures, relaxation may be blocked as a consequence of freezing secondary β-relaxations. One may conclude that the current range of validity of our physical description correspond to temperatures higher than 340 K ($T_g - 33$ K) or relaxation times shorter than 10^5-10^6 s.

Currently, we only describe the equilibrium temperature dependence of ξ. The arguments in reference[14] show that ξ depends on the whole "bare" distribution of relaxation times. In principle, ξ should increase as the aging time increases. We assume a constant ξ value close to that estimated at T_g in various non polar polymers, because the dynamical states we consider remain relatively close to T_g. The dependence of ξ might be studied by investigating the diffusion of small fluorescent probes in polymers with different thermo-mechanical histories, as it has been done the group of Ediger.[11,18] Such experimental data, however, are currently not available.

It is important to note that the free energy barrier changes on the monomer scale are

indeed very small, of the order of $10^{-2}k_BT$. However, on the scale ξ which involves a number $N_c \sim 1000$ of monomers, this results on large changes of free energy barriers, of the order of $N_c \times 10^{-2}k_BT \sim 10k_BT$. The free energy barrier for collective reorganization within a subunit leading to the creation of one hole allowing for α-relaxation is reduced by this amount, which explains why the yield stress is so low in glassy polymers. This aspect is at the very heart of our theory[48,51] and has been discussed in reference.[50]

The evolution of the tensorial element q_{33} in the tensile direction is quantitatively comparable to the results obtained by Vogt et al by NMR, with a value of q_{33} of the order of 0.2 in polycarbonate at 100% of deformation.[72] Many other studies have observed optical anisotropy but comparison can only be qualitative because the monomer optical anisotropy is usually not known quantitatively.[75–77] Further studies should aim at measuring the evolution of the orientation during various thermo-mechanical experiments in order to check the validity of the theory and to further quantify the values of the adjustable parameters.

Other approaches have been proposed to describe strain hardening and the associated effects. Hoy and O'Hern[42] have introduced a dynamical equation for the evolution of large scale chain orientation under deformation. Large chain orientation relaxes slowly, with a relaxation time scaling as the molecular weight N of the chains during deformation and as N^2 upon cessation of the flow. In the model by Hoy and O'Hern, the increase of the stress in the strain hardening regime is a direct effect of chain orientation and the associated increase of the size of plastic event correlation zones. Memory effects are incorporated in the model as a consequence of the slow relaxation of large scale chain orientation. Strain hardening has been recently studied by coarse-grained molecular dynamics simulations by Zou et al.[78,79] However, these authors do not describe yield and plastic flow itself. Their model does not predict changes in the relaxation times.

Our model is consistent with the MD results and analysis by Hoy and Robbins.[29,31,42]

Indeed, Hoy and Robbins concluded that the stress and the dissipation due to relaxation events in the strain hardening regime are of the same nature as those observed at yield and during flow stress. At this regard, our theory is fully compatible with their results, as we propose that these same interactions are at play, with longer lifetimes, in the strain hardening regime. Following the work by Hoy and Robbins, the Haward's and all similar models which involve entropic elasticity between entanglements are inconsistent with Hoy and Robbins interpretation of their simulations. In contrast, in the present work, we show that the acceleration of the dynamics up to yield and during stress softening followed by an increase of relaxation times during strain hardening, as well as the corresponding non-monotonic evolution of the β parameter in these regimes of deformation, are key features of the plastic deformation and strain hardening of glassy polymers.[18,19,26,27] On the other hand, strain hardening is indeed associated to high molecular weight polymers. Our point of view is that chain ends act like defects which prevent local orientation in their neighborhood and thereby prevent strain hardening to take place. We do not consider chain ends in our model for the moment and implicitly assume that their role is negligible, which corresponds to the case of high molecular weight polymers. Considering the effect of chain ends and how they suppress strain hardening for shorter polymers will be a further extension of our theory.

The theoretical description proposed here for strain hardening is consistent with other aspects of the theoretical model developped in.[14,48,49,51,56–58,69] In particular, the length scale ξ of 3-5 nm is the same as the one used for explaining T_g shifts in thin films,[49,56,69] the reinforcement of filled elastomers[80–83] and the violation of the Stokes law for small probe diffusion in polymers in the vicinity of T_g.[14] The facilitation mechanism which is responsible for this length scale[14,45] also explains the temporal asymmetry between aging and rejuvenation,[58] a feature confirmed by Medvedev and Caruthers.[84] The same facilitation mechanism is used in this manuscript and is responsible for the narrowing of the distribution of relaxation times at yield and in the stress softening regime.[51] Other defining features of the physics of

strain hardening in glassy polymers include the Bauschinger memory effects[5,43,53,85,86] measured in mechanical experiments and by dielectric spectroscopy[26–28] or by using fluorescent probes.[18–20] Note also that DSC measurements by Hasan and Boyce have shown that predeformation in the strain hardening regime modifies the subsequent DSC response even above T_g,[87] whereas smaller predeformations below the strain hardening threshold affects the DSC response below T_g only. A complete theory of polymer plasticity will eventually have to explain and reproduce the whole observed complex behavior in a consistent and unified way.

In conclusion, we have introduced a microscopic model for strain hardening, in which a key assumption is that free energy barriers associated to α-relaxation are set on a scale of $N_c \sim 1000$ monomers. Strain hardening and associated distinctive features are explained in a unified way. The model allows obtaining not only strain-stress curves consistent with experimental data, but also evolutions of the dominant relaxation time and of the width of the distribution of relaxation times during the course of deformation which are, at least semi-quantitatively, in agreement with recent experimental results.

Acknowledgments

Sergio Ciliberto and Caroline Crauste-Thibierge acknowledge support by the Région Auvergne-Rhône Alpes via the contract DyLoFiPo

BIBLIOGRAPHY

References

(1) Ferry, J. D. *Viscoelastic Properties of Polymers*; John Wiley and Sons, Inc., 1980.

(2) Nielsen, L. E.; Landel, R. F. *Mechanical Properties of Polymers and Composites*; Marcel Dekker, New York, 1994.

(3) Meijer, H.; Govaert, L. Multi-scale analysis of mechanical properties of amorphous polymer systems. *Macromolecular Chemistry and Physics* **2003**, *204*, 274–288.

(4) Haward, R. *The Physics of Glassy Polymers*; Applied Science Publishers, London, 1973.

(5) Klompen, E. T. J.; Engels, T. A. P.; Govaert, L. E.; Meijer, H. E. H. Modeling of the postyield response of glassy polymers: Influence of thermomechanical history. *Macromolecules* **2005**, *38*, 6997–7008.

(6) Meijer, H. E. H.; Govaert, L. E. Mechanical performance of polymer systems: The relation between structure and properties. *Prog. Polym. Sci.* **2005**, *30*, 915–938.

(7) Van Melick, H.; Meijer, H.; Govaert, L. On the origin of strain hardening in glassy polymers. *Polymer* **2003**, *44*, 2493–2502.

(8) Charvet, A.; Vergelati, C.; Sotta, P.; Long, D. R. Damage Mechanisms of Plasticized Cellulose Acetate under Tensile Deformation Studied by Ultrasmall-Angle X-Ray Scattering. *Macromolecules* **2019**, *52*, 6613–6632.

(9) Djukic, S.; Bocahut, A.; Bikard, J.; Long, D. R. Study of Damage Mechanisms of Amorphous and Low Semicrystalline Polymers under Tensile Deformation by Ultrasmall-Angle X-ray Scattering. *Macromolecules* **2020**, *53*, 5538–5529.

(10) Ediger, M. D.; Angell, C. A.; Nagel, S. R. Supercooled liquids and glasses. *J. Phys. Chem* **1996**, *100*, 13200–13212.

(11) Ediger, M. Spatially heterogeneous dynamics in supercooled liquids. *Annu. Rev. Chem.* **2000**, *51*, 99–128.

(12) Tracht, U.; Wilhelm, M.; Heuer, A.; Feng, H.; Schmidt-Rohr, K.; Spiess, H. Length scale of dynamic heterogeneities at the glass transition determined by multidimensional nuclear magnetic resonance. *Phys. Rev. Lett.* **1998**, *81*, 2727 – 2730.

(13) Cicerone, M. T.; Blackburn, F. R.; Ediger, M. D. Anomalous diffusion of probe molecules in polystyrene - Evidence for spatially heterogeneous segmental dynamics. *Macromolecules* **1995**, *28*, 8224 – 8232.

(14) Merabia, S.; Long, D. Heterogeneous dynamics in van der Waals liquids. Determination of the characteristic scale. *Eur. Phys. J. E* **2002**, 195–207.

(15) Crauste-Thibierge, C.; Brun, C.; Ladieu, F.; L'Hôte, D.; Biroli, G.; Bouchaud, J.-P. Evidence of Growing Spatial Correlations at the Glass Transition from Nonlinear Response Experiments. *Phys. Rev. Lett.* **2010**, *104*, 165703.

(16) Masurel, R.; Cantournet, S.; Dequidt, A.; Long, D.; Montes, H.; Lequeux, F. Linear Viscoelasticity of polymer in their glass transition domains : 2d finite elements simulations. *Macromolecules* **2015**, *48*, 6690–6702.

(17) Loo, L. S.; Cohen, R. E.; Gleason, K. K. Chain Mobility in the Amorphous Region of Nylon 6 Observed under Active Uniaxial Deformation. *Science* **2000**, *288*, 116–119.

(18) Lee, H.-N.; Paeng, K.; Swallen, S. F.; Ediger, M. D. Direct Measurement of Molecular Mobility in Actively Deformed Polymer Glasses. *Science* **2009**, *323*, 231–234.

(19) Lee, H.-N.; Riggleman, R. A.; de Pablo, J. J.; Ediger, M. D. Deformation-Induced Mobility in Polymer Glasses during Multistep Creep Experiments and Simulations. *Macromolecules* **2009**, *42*, 4328–4336.

(20) Lee, H.-N.; Paeng, K.; Swallen, S.; Ediger, M.; Stamm, R.; Medvedev, G.; Caruthers, J. Molecular Mobility of Poly(methyl methacrylate) Glass During Uniaxial Tensile Creep Deformation. *J. Polym. Sci.: Polym. Phys. Ed.* **2009**, *47*, 1713–1727.

(21) Kalfus, J.; Detwiler, A.; Lesser, A. J. Probing Segmental Dynamics of Polymer Glasses during Tensile Deformation with Dielectric Spectroscopy. *Macromolecules* **2012**, *45*, 4839–4847.

(22) Perez-Aparicio, R.; Cottinet, D.; Crauste-Thibierge, C.; Vanel, L.; Sotta, P.; Delannoy, J.-Y.; Long, D. R.; Ciliberto, S. Dielectric spectroscopy of a stretched polymer glass: heterogeneous dynamics and plasticity. *Macromolecules* **2016**, *49*, 3889–3898.

(23) Bending, B.; Christison, K.; Ricci, J.; Ediger, M. D. Measurement of Segmental Mobility during Constant Strain Rate Deformation of a Poly(methyl methacrylate) Glass. *Macromolecules* **2014**, *47*, 800 – 806.

(24) Hebert, K.; Ediger, M. Reversing Strain Deformation Probes Mechanisms for Enhanced Segmental Mobility of Polymer Glasses. *Macromolecules* **2017**, *50*, 1016–1026.

(25) Bennin, T.; Ricci, J.; Ediger, M. Enhanced Segmental Dynamics of Poly(lactic acid) Glasses during Constant Strain Rate Deformation. *Macromolecules 2020* **2019**, *52*, 6428–6437.

(26) Sahli, R.; Hem, J.; Crauste-Thibierge, C.; Clement, F.; Long, D. R.; Ciliberto, S. Relaxation time of a polymer glass stretched at very large strains. *Phys. Rev. Mater.* **2020**, *4*, 035601.

(27) Hem, J.; Crauste-Thibierge, C.; Clément, F.; Long, D. R.; Ciliberto, S. Simultaneous memory effects in the stress and in the dielectric susceptibility of a stretched polymer glass. *Phys. Rev. E* **2021**, *103*, L040502.

(28) Hem, J.; Merlette, T.; Crauste-Thibierge, C.; Clément, F.; Long, D. R.; Ciliberto, S. Microscopic Dynamics in the Strain Hardening Regime of GlassyPolymers. *Macromolecules* **2022**, *55*, 9168–9185.

(29) Hoy, R. S.; Robbins, M. O. Strain hardening in polymer glasses: Limitations of network models. *Physical Review Letters* **2007**, *99*, 117801.

(30) Hoy, R. S.; Robbins, M. O. Scaling of the Strain Hardening Modulus of Glassy Polymers with the Flow Stress. *Polymer Physics* **2009**, *47*, 1406–1411.

(31) Hoy, R. S.; Robbins, M. O. Strain Hardening of Polymer Glasses: Entanglements, Energetics, and Plasticity. *Physical Review E* **2008**, *77*, 031801.

(32) Hoy, R. Why is Understanding Glassy Polymer Mechanics So Difficult? *Journal of polymer science. Part B. Polymer physics* **2011**, *49*, 979–984.

(33) Hoy, R. *Polymer Glasses. Chapter: Modeling strain hardening in polymer glasses using molecular simulations. pp 425-450*; Taylor and Francis Group: Boca Raton, Editor C. B. Roth, 2016.

(34) Haward, R. Strain hardening of thermoplastics. *Macromolecules* **1993**, *26*, 5860–5869.

(35) Riggleman, R. A.; Lee, H.-N.; Ediger, M. D.; de Pablo, J. J. Heterogeneous dynamics during deformation of a polymer glass. *Soft Matter* **2010**, *6*, 287 – 291.

(36) Riggleman, R. A.; Lee, H.-N.; Ediger, M. D.; de Pablo, J. J. Free Volume and Finite-Size Effects in a Polymer Glass under Stress. *Phys. Rev. Lett.* **2007**, *99*, 215501.

(37) Tsamados, M.; Tanguy, A.; Goldenberg, C.; Barrat, J.-L. Local elasticity map and plasticity in a model Lennard-Jones glass. *Phys. Rev. E* **2009**, *80*, 026112.

(38) Papakonstantopoulos, G.; Riggleman, R.; Barrat, J.-L.; de Pablo, J. Molecular plasticity of polymeric glasses in the elastic regime. *Phys. Rev. E* **2008**, *77*, 041502.

(39) Barrat, J.-L.; Baschnagel, J.; Lyulin, A. Molecular dynamics simulations of glassy polymers. *Soft Matter* **2010**, *6*, 3430–3446.

(40) Lyulin, A.; Vorselaars, B.; Mazo, M.; Michels, M. Strain softening and hardening of amorphous polymers: Atomistic simulation of bulk mechanics and local dynamics. *Europhys. Lett.* **2005**, *71*, 618–624.

(41) Vorselaars, B.; Lyulin, A.; Michels, M. Microscopic Mechanisms of Strain Hardening in Glassy Polymers. *Macromolecules* **2009**, *42*, 5829–5842.

(42) Hoy, R. S.; O'Hern, C. S. Viscoplasticity and large-scale chain relaxation in glassy-polymeric strain hardening. *Physical Review E* **2010**, *82*, 041803.

(43) Ge, T.; Robbins, M. O. Anisotropic plasticity and chain orientation in polymer glasses. *Journal of Polymer Science Part B: Polymer Physics* **2010**, *48*, 1473–1482.

(44) Chen, K.; Schweizer, K. S. Stress-enhanced mobility and dynamic yielding in polymer glasses. *Europhysics Letters* **2007**, *79*, 26006.

(45) Chen, K.; Saltzman, E.; Schweizer, K. Segmental dynamics in polymers: from cold melts to ageing and stressed glasses. *J. Phys. : Condens. Matter* **2009**, *21*, 503101.

(46) Chen, K.; Schweizer, K. S. Suppressed Segmental Relaxation as the Origin of Strain Hardening in Polymer Glasses. *Phys. Rev. Lett.* **2009**, *102*, 038301.

(47) Chen, K.; Schweizer, K. Theory of Yielding, Strain Softening, and Steady Plastic Flow in Polymer Glasses under Constant Strain Rate Deformation. *Macromolecules* **2011**, *44*, 3988–4000.

(48) Dequidt, A.; Long, D.; Sotta, P.; Sanseau, O. Mechanical properties of thin confined polymer films close to the glass transition in the linear regime of deformation: Theory and simulations. *Eur. Phys. J. E* **2012**, *35*, 61.

(49) Dequidt, A.; Conca, L.; Delannoy, J.; Sotta, P.; Lequeux, F.; Long, D. Heterogeneous Dynamics and Polymer Plasticity. *Macromolecules* **2016**, *49*, 9148–9162.

(50) Long, D.; Conca, L.; Sotta, P. Dynamics in glassy polymers: The Eyring model revisited. *Phys. Rev. Mater.* **2018**, *2*, 105601.

(51) Conca, L.; Dequidt, A.; Sotta, P.; Long, D. R. Acceleration and Homogenization of the Dynamics during Plastic Deformation. *Macromolecules* **2017**, *50*, 9456–9472.

(52) Belguise, A.; Cantournet, S.; Lequeux, F.; Montes, H. Weak nonlinearities in viscoelastic mechanical properties of polymers near their glass transition: Local versus macroscopic laws for stress-induced acceleration of the mechanical response. *Phys. Rev. M* **2021**, *5*, 33601.

(53) Senden, D.; van Dommelen, J.; Govaert, L. Strain Hardening and Its Relation To Bauschinger Effects in Oriented Polymers. *Journal of Polymer Science Part B: Polymer Physics* **2010**, *48*, 1483–1494.

(54) Senden, D. J. A.; Krop, S.; van Dommelen, J. A. W.; Govaert, L. E. Rate- and Temperature-Dependent Strain Hardening of Polycarbonate. *Journal of Polymer Science Part B: Polymer Physics* **2012**, *50*, 1680–1693.

(55) Merlette, T. *Theory of strain hardening of glassy polymers*; PhD thesis, Lyon, 2022.

(56) Long, D.; Lequeux, F. Heterogeneous dynamics at the glass transition in van der Waals liquids, in the bulk and in thin films. *Eur. Phys. J. E* **2001**, *4*, 371–387.

(57) Merabia, S.; Long, D. R. Heterogeneous dynamics and pressure dependence of the dynamics in van der Waals liquids. *Macromolecules* **2008**, *41*, 3284–3296.

(58) Merabia, S.; Long, D. Heterogeneous dynamics, ageing, and rejuvenating in van der Waals liquids. *J. Chem. Phys.* **2006**, *125*, 234901.

(59) Garrahan, J. P.; Chandler, D. Geometrical explanation and scaling of dynamical heterogeneities in glass forming systems. *Phys. Rev. Lett.* **2002**, *89*, 035704.

(60) Ritort, F.; Sollich, P. Glassy dynamics of kinetically constrained models. *Advances in Physics* **2003**, *52*, 219–342.

(61) Kovacs, A. J. Glass transition in amorphous polymers: a phenomenological study. *J. Polym. Sci.* **1958**, *30*, 131–147.

(62) Doi, M.; Edwards, S. *The Theory of Polymer Dynamics*; Oxford Science Publications, Oxford, 1986.

(63) De Gennes, P.-G.; Prost, J. *Physics of liquid crystals*; Oxford Science Publications, Oxford, 1994.

(64) Semenov, A. Rheological properties of a nematic solution of semiflexible macromolecules. *Sov. Phys. JETP* **1987**, *66*, 712–716.

(65) Long, D.; Morse, D. A Rouse-like model of liquid crystalline polymer melts: Director dynamics and linear viscoelasticity. *J. Rheology* **2002**, *46*, 49–92.

(66) Flory, P. *Macromolecules*; Oxford, 1956.

(67) van Breemen, L.; Engels, T.; Klompen, E.; Senden, D.; Govaert, L. Rate- and Temperature-Dependent Strain Softening in Solid Polymers. *J. Polym. Sci. Part B: Polym. Phys.* **2019**, *50*, 1589–1596.

(68) Sotta, P.; Long, D. Crosss-over from 2D to 3D percolation. *Eur. Phys. J. E* **2003**, *11*, 375–388.

(69) Merabia, S.; Sotta, P.; Long, D. Heterogeneous dynamics in van der Waals liquids and glass transition in confinement. *Eur. Phys. J. E* **2004**, *15*, 189–210.

(70) Struik, L. C. E. *Physical Aging in Amorphous Polymers and Other Materials*; Elsevier, Oxford, 1978.

(71) Wendlandt, M.; Tervoort, T. A.; Suter, U. W. Strain-hardening modulus of cross-linked glassy poly(methyl methacrylate). *Journal of Polymer Science Part B: Polymer Physics* **2010**, *48*, 1464–1472.

(72) Vogt, V.-D.; Dettenmaier, M.; DSpiess, H.; Pietralla, M. Orientation of the diphenylene propane unit in stretched polycarbonate from two-dimensional magic-angle-spinning NMR. *Colloid Polym. Sci.* **1990**, *268*, 22–27.

(73) Parsegian, V. A. *Van der Waals Forces*; Cambridge University Press, Cambridge, 2006.

(74) Medvedev, G.; Caruthers, J. Development of a stochastic constitutive model for prediction of postyield softening in glassy polymers. *J. Rheology* **2013**, *57*, 949–1002.

(75) Botto, P. A.; Duckett, R. A.; Ward, I. M. The yield and thermoelastic properties of oriented poly(methyl methacrylate). *Polymer* **1987**, *28*, 257–262.

(76) Rawson, F. F.; Rider, J. G. A. Correlation Of Young's Modulus With Yield Stress In Oriented Poly(Vinyl Chloride). *Polymer* **1973**, *15*, 107–110.

(77) Inoue, T.; Okamoto, H.; Osaki, K. Birefringence of Amorphous Polymers. 1. Dynamic Measurement on Polystyrene. *Macromolecules* **1991**, *24*, 570–575.

(78) Zou, W.; Larson, R. A hybrid Brownian dynamics/constitutive model for yielding, aging, and rejuvenation in deforming polymeric glasses. *Soft Matter* **2016**, *12*, 6757–6770.

(79) Zou, W.; Moghadam, S.; Hoy, R.; Larson, R. Multiscale Modeling of Sub-Entanglement-Scale Chain Stretching and Strain Hardening in Deformed Polymeric Glasses. *Macromolecules* **2019**, *52*, 9248–9260.

(80) Berriot, F., J.and Lequeux; Monnerie, L.; Montes, H.; Sotta, P.; Long, D. Filler-elastomer interaction in model filled rubbers, a ^{1}H NMR study. *J. Non Crystalline Solids* **2002**, *307*, 719–724.

(81) Berriot, J.; Montes,; Lequeux, F.; Long, D.; Sotta, P. Evidence for the Shift of the Glass Transition near the Particles in Silica-Filled Elastomers. *Macromolecules* **2002**, *35*, 9756–9762.

(82) Berriot, J.; Sotta, P.; Long, D.; Montes,; Lequeux, F. Gradient of glass transition temperature in filled elastomers. *Europhysics Letters* **2003**, *64*, 50–56.

(83) Merabia, S.; Sotta, P.; Long, D. R. A Microscopic Model for the Reinforcement and the Nonlinear Behavior of Filled Elastomers and Thermoplastic Elastomers (Payne and Mullins Effects). *Macromolecules* **2008**, *41*, 8252–8266.

(84) Medvedev, G.; Caruthers, J. Predictions of Volume Relaxation in Glass Forming Materials Using a Stochastic Constitutive Model. *Macromolecules* **2015**, *48*, 788–800.

(85) Arruda, M. C., E. M.; Boyce Evolution of plastic anisotropy in amorphous polymers during finite straining. *International Journal of Plasticity* **1993**, *9*, 697–720.

(86) Arruda, M. C., E. M.; Boyce Effects of initial anisotropy on the finite strain deformation behavior of glassy polymers. *International Journal of Plasticity* **1993**, *9*, 783–811.

(87) Hasan, O. A.; Boyce, M. C. Energy storage during inelastic deformation of glassy polymers. *Polymer* **1993**, *34*, 5085–5092.